Ionospheric effects of 5–6 January 2019 eclipse over the People's Republic of China: Results from oblique sounding

Leonid F. Chernogor[1, 2, 3], Kostyantyn P. Garmash[1], Qiang Guo[2], Victor T. Rozumenko[1], Yu Zheng[3]

[1]Department of Space Radio Physics, V. N. Karazin Kharkiv National University, 4 Svobody Sq., Kharkiv, 61022, Ukraine
[2]College of Information and Communication Engineering, Harbin Engineering University, 145 Nantong Street, Nangang District, Harbin, 150001, China
[3]College of Electronic Information, Qingdao University, 308 Ningxia Road, Qingdao, 266071, China

Correspondence to: Yu Zheng (zhengyu@qdu.edu.cn)

Bullet points:

The solar eclipse was accompanied by up to ±1.5 Hz Doppler spectrum broadening and ±0.5 Hz variations in the Doppler shift, f_D.

Atmospheric gravity waves excited 15 min period variations in f_D and 1.6 – 2.4 % perturbations in N.

Infrasound excited 4–5 min period variations in f_D and 0.2 – 0.3 % perturbations in N.

The greatest decrease in the ionospheric electron density, N, attains –15 %, whereas the theoretical estimate is –13 %.

1

Abstract. The paper deals with the variations in the Doppler spectra and in the relative amplitudes of the signals observed at oblique incidence over the People's Republic of China (PRC) during the partial solar eclipse of 5–6 January 2019 and on reference days. The observations were made using the multifrequency multiple path radio system for sounding the ionosphere at oblique incidence. The receiver system is located at the Harbin Engineering University campus, PRC, and 14 HF broadcasting station transmitters are used for taking measurements along the Lintong/Pucheng to Harbin, Hwaseong to Harbin, Chiba/Nagara to Harbin, Hailar/Nanmen to Harbin, Beijing to Harbin (three paths), Goyang to Harbin, Ulaanbaatar/Khonkhor to Harbin, Yakutsk to Harbin (two paths), Shijiazhuang to Harbin, Hohhot to Harbin, and Yamata to Harbin radio wave propagation paths. The specific feature of this partial solar eclipse was that it occurred during local time morning with a geomagnetic disturbance ($K_p \approx 3-$) in the background. The response of the ionosphere to the solar eclipse has been inferred from temporal variations in the Doppler spectra, the Doppler shift, and the signal relative amplitude. The partial solar eclipse was found to be associated by Doppler spectrum broadening, up to ±1.5 Hz, alternating sign Doppler shift variations, up to ±0.5 Hz, in the main ray, and by quasi-periodic Doppler shift changes. The relative amplitude of electron density disturbances in the 15 min period atmospheric gravity wave field and in the 4–5 min period infrasound wave field is estimated to be $1.6 - 2.4$ % and $0.2 - 0.3$ %, respectively. The estimates of a maximum decrease in the electron density are in agreement with the observations.

1 Introduction

A solar eclipse is quite a rare natural phenomenon. The maximum phase of a total eclipse can persist for a fraction of a second to a maximum of 7 min 32 s, whereas a partial solar eclipse persists for about 2–3 h. The umbra's path width varies from ~150 km at the equator to 1,000 km at the poles, and the Moon's shadow travels at a speed of about 500 to 1,000 m/s, depending on the geographic latitude (Chernogor, 2013a).

A solar eclipse acts to significantly modify energy influx, capable of producing variations in all geophysical fields, changes in the parameters of the processes acting in the sub-systems of the Earth (internal spheres)–atmosphere–ionosphere–magnetosphere (EAIM) system, and disrupting the existing couplings between the subsystems (Chernogor, 2003, 2011; Chernogor and Rozumenko, 2008). The processes caused by a solar eclipse in the EAIM system are resembling the processes observed to occur at the morning-evening meridian, but they differ from the latter both quantitatively and qualitatively. First, the changes in the solar energy flux during a solar eclipse occur at an almost unchanging zenith angle (it changes only by $8 - 12\%$). Second, the effects of a solar eclipse in the EAIM system depend significantly on season, local time, the state of atmospheric and space weather, etc. Moreover, unlike the terminator, the Moon's shadow moves at supersonic speed. All these factors make each eclipse one of a kind. The study of the EAIM system response to a solar eclipse permits the establishment of direct and reverse, positive and negative couplings between the subsystems, the

2

specification of physical and chemical processes operating in the subsystems, and the determination of a number of parameters of these processes, etc. (Chernogor, 2003, 2011; Chernogor and Rozumenko, 2008).

55   Astronomers have been studying solar eclipses for thousands of years. The study of the upper atmosphere and ionosphere began in the twentieth century, encompassing the effects that a solar eclipse has on these media. First attempts to observe effects arising during a solar eclipse date back to the 1930 – 1940s (see, e.g., Chapman, 1932; Higgs, 1942). An eclipse-related distortion of the radio wave characteristics was used first, and then the ionosonde technique. The first collection of papers dealing with ionospheric effects of solar eclipses was published during the 1950s (Beynon and Brown, 60   1956).

       The investigation of processes caused by solar eclipses became especially active with the advent of the space age when a broad spectrum of rocket and satellite measurements found applications in the field. The incoherent scatter radar, the single most powerful ground-based technique for probing geospace, appeared at the same time. During the 1970s and later, the study of processes caused by eclipses became more active. Astronomical, radio, satellite, and other techniques were used 65   for this purpose, which were described in special issues of journals (see, e.g., Eclipse Supplement …, 1970; Journal …, 1972) or in books (see, e.g., Anastassiades, 1970).

       The study of the ionospheric response to solar eclipses has advanced dramatically in the past 40 years. One should acknowledge that the manifestation of the ionospheric effects is dependent on many factors, including the measurement techniques. Thus, the involvement of techniques other than the conventional techniques (ionosonde, incoherent scatter radar, 70   satellite radio beacon receivers, etc.) would be appropriate, including the technique used in this study. The important feature of the ionospheric response to note is that there are no two identical reactions to two similar solar eclipses. Therefore, the authors have restricted their review only to a listing of the main works in the field. The studies conducted by Chandra et al. (1980, Sen Gurta et al. (1980), Deshpande et al. (1982), Rama Rao et al. (1982), Roble et al. (1986), Salah et al. (1986), and Liu et al. (1998) during the 1980 – 1990s should be noted. Results obtained in recent two decades are presented in the studies 75   by Uryadov et al. (2000), Akimov et al. (2005), Burmaka et al. (2006a, 2006b), Founda et al. (2007), Afraimovich et al. (2007), Šauli et al. (2007), Special… (2007), Jakowski et al. (2008), Grigorenko et al. (2008), Lyashenko and Chernogor (2008), Akimov and Chernogor (2010), Chernogor (2010a, 2010b, 2012a, 2012b, 2013b, 2016a, 2016b), Garmash et al. (2011), Marlton et al. (2016), Uryadov et al. (2016), Verhulst et al. (2016), Stankov et al. (2017), Chernogor and Garmash (2017), Coster et al. (2017), Chernogor et al. (2019).

80   Some eclipses attracted particular attention. Recent work (Chernogor, 2012a, 2012b, 2013b, 2016a, 2016b; Marlton et al., 2016; Uryadov et al., 2016; Verhulst et al., 2016; Chernogor and Garmash, 2017; Stankov et al., 2017; Chernogor et al., 2019; Panasenko et al., 2019) describes ionospheric effects of the solar eclipse of 29 March 2015 in Europe. Coster et al. (2017) analyze effects of the solar eclipse of 21 August 2017. Guo et al. (2020) discuss the effects of the partial solar eclipse of 11 August 2018 in the ionosphere over the PRC. The observations have been made with the coherent multi-frequency 85   multiple path radio system, the receiver of which is located at the Harbin Engineering University campus and 14 transmitters are situated in the PRC, Japan, Mongolia, the Republic of Korea, and the Russian Federation. In the ionosphere, aperiodic

3

and quasi-periodic perturbations in the electron density, N, have been detected with a 1–10% amplitude and a ~10-min period, T, whereas the decrease in the ionospheric E region electron density attains 26%, which agree well with the theoretical estimate (24%). The solar eclipse of 21 June 2020 that occurred in the equatorial ionosphere was observed by Le et al. (2020), Zhang et al. (2020), Huang et al. (2020, 2021), Dang et al. (2020), Patel and Singh (2021), Wang et al. (2021a, 2021b), Şentürk et al. (2021), Sun et al. (2021), Shagimuratov et al. (2021), Aa et al. (2021), Chen et al. (2021), Tripathi et al. (2022); the ionospheric effects were observed to occur with the South Atlantic Anomaly in the background. Zhang et al. (2020) detected effects from the solar eclipse in the magnetically conjugate region. Chernogor and Mylovanov (2022) describe the ionospheric effects of the annular solar eclipse of 10 June 2021 that occurred in the high latitudes. The atmospheric, ionospheric, and magnetic effects of this eclipse are analyzed by Chernogor (2021a, 2021b, 2022), Chernogor and Mylovanov (2022), Chernogor and Garmash (2022).

More recently, increasingly sophisticated models have been developed. Based on the observations of two eclipses, Verhulst and Stankov (2020) analyzed the altitude dependence of the ionospheric effects from solar eclipses. Based on the solar eclipse of 21 August 2017, Mrak et al. (2022) have studied the contribution of the ultraviolet emissions from the solar corona to the ionization of the atmosphere and determined that the value of this contribution could attain a factor of 0.2 the total rate of ionization.

The regular effects, such as a decrease in the electron density, and in the electron and ion temperatures, variations in the ion composition, and vertical plasma movements have so far been studied quite well (see, e.g., Akimov et al., 2005; Burmaka et al., 2006a, 2006b; Grigorenko et al., 2008; Lyashenko and Chernogor, 2008; Chernogor, 2012a, 2012b, 2013a, 2013b, 2016a, 2016b; Chernogor et al., 2019; Panasenko et al., 2019). The irregular effects, which may differ for different eclipses, have been studied significantly less (Akimov et al., 2005; Burmaka et al., 2006a, 2006b; Grigorenko et al., 2008; Lyashenko and Chernogor, 2008; Akimov and Chernogor, 2010; Chernogor, 2010a, 2010b, 2012a, 2012b, 2013b; Garmash et al., 2011; Marlton et al., 2016; Chernogor and Garmash, 2017; Stankov et al., 2017; Coster et al., 2017). The generation of wave perturbations, which was foretold by Chimonas and Hines (1970), also belong to these effects. At present, the problem of studying the response of all Earth's spheres to solar eclipses has become an interdisciplinary subject. In addition to astronomers and physicists, meteorologists, medical doctors (ophthalmologists, optometrists, and even psychiatrists), sociologists, biologists, ecologists, etc. have joined the study of the subject.

Thus, a lot of observations have been made of the effects that solar eclipses have on the ionosphere over one hundred years of eclipse subject history. Nevertheless, the study of these effects remains an urgent problem. There are a few reasons for this. First, solar eclipses take place in the different regions of the world, whereas the physical processes operating in the low- and high-latitude ionosphere differ considerably, and consequently the responses to solar eclipses in the low-, mid-, and high-latitude ionosphere also differ from place to place. Second, the response mentioned above is largely dependent on the state of atmospheric and space weather. Third, the ionospheric response is notably dependent on the eclipse onset. Fourth, the ionospheric response depends on the phase of the eclipse and on its duration. Finally, the application of different techniques for probing the ionosphere permits the addition of extra information on the ionospheric effects of solar

4

eclipses and allows the revelation of new details in these effects. All these factors indicate the specific features of each solar eclipse. Along with regular features, the ionospheric response has specific features that are characteristic of the given solar eclipse, which explain the urgency of this work. The purpose of this work is to present the observations of variations in the Doppler spectra and in the amplitudes of radio waves that travelled along oblique propagation paths over the PRC in the

125   course of the partial solar eclipse of 5/6 January 2019 UT period and on the previous and next days. The description of the experiment is followed by the theoretical estimates of variations in the electron density during the solar eclipse and a comparison with the observations.

2 The state of space weather

A preliminary analysis of the state of space weather is needed to correctly select the effects from the solar eclipse. The

130   proton density, n_{sw}, in the solar wind plasma exhibited a gradual increase from 2×10^6 m^{-3} on 3 January 2019 to 30×10^6 m^{-3} at 20:00 UT on 4 January 2019 (Figure 1), whereas during 4–5 January 2019, it showed a gradual decrease to the initial level of approximately 2×10^6 m^{-3} (Retrieved from https://omniweb.gsfc.nasa.gov/form/dx1.html). The flow speed, V_{sw}, of the solar wind plasma showed a gradual increase from 300 km/s on 4 January 2019 to 552 km/s at 17:00 UT on 6 January 2019. The proton temperature in the solar wind plasma exhibited the greatest changes during 4–5 January 2019, when it showed an

135   increase from 10^4 K on 4 January 2019 to 2.9×10^5 K at 08:00 UT on 5 January 2019. The increases in n_{sw} and V_{sw} observed on 4 January 2019 resulted in an increase in the dynamic pressure, p_{sw}, from $0.2 - 0.3$ nPa to $6 - 7$ nPa (see Figure 1).

The interplanetary magnetic field B_y component showed variability within the ± 5 nT limits during 4–5 January 2019. The B_z component exhibited variations from 0 nT to –5 nT after approximately 04:00 UT on 4 January 2019 and to the end of the day, whereas the Akasofu function showed an increase to 8GJ/s, which triggered a moderate magnetic storm that

140   persisted from 16:00 UT on 4 January 2019 and to the end of 5 January 2019, when the geomagnetic K_p index attained a maximum, $K_{p\max}$, of 5, and the equatorial D_{st} index attained a minimum, $D_{st\min}$, of –23 nT at approximately 16:00 UT on 5 January 2019. The magnetic field perturbation, $K_p \approx 3$, took place on 6 January 2019, when the value of the D_{st} index did not exceed –10 nT.

Table 1 presents the daily 10.7 cm solar flux, which is used as a measure of solar activity.

145   In general, the states of solar activity and space weather were favorable for the observations of ionospheric effects from the partial solar eclipse of 6 January 2019 local time over the PRC.

150

Table 1. Daily $F_{10.7}$ index for the 2–8 January 2019 UT period.

Date (January 2019)	02	03	04	05	06	07	08
$F_{10.7}$	72.7	70.2	69.1	68.8	69.6	69.1	69.0
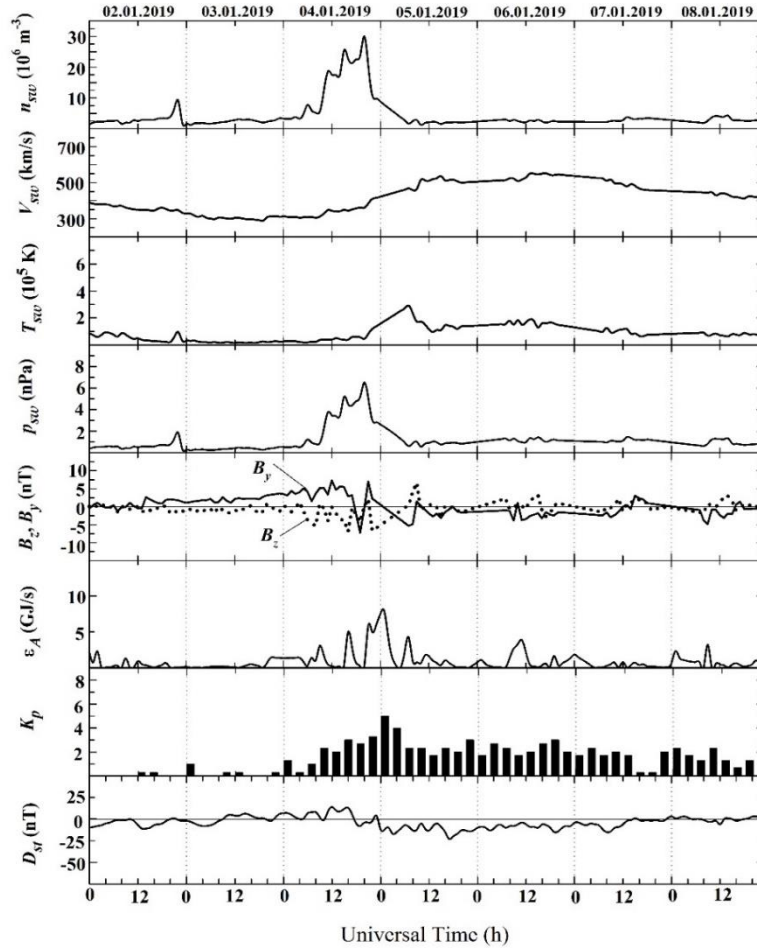
Figure 1. Universal time dependencies of the solar wind parameters: observed proton number density n_{sw}, plasma speed V_{sw}, and temperature T_{sw}; calculated dynamic pressure p_{sw}; measured B_z and B_y components of the interplanetary magnetic field; estimated energy input, ε_A, into the Earth's magnetosphere from the solar wind per unit time; and K_p- and D_{st}-indices for the 2–8 January 2019 period. Dates are shown along the upper abscissa axis. Experimental data are retrieved from https://omniweb.gsfc.nasa.gov/form/dx1.html

6

3 Instrumentation

The observations of the effects from the solar eclipse were made with the multi-frequency multiple path radio system designed to probe the ionosphere obliquely. The system developed in collaboration between researchers from the V. N. Karazin Kharkiv National University (Ukraine) and the Harbin Engineering University (PRC) consists of the receiver system located at the Harbin Engineering University campus (45.78°N, 126.68°E) and 14 broadcasting stations in the PRC, Japan, Mongolia, the Republic of Korea, and the Russian Federation. The system continuously monitored dynamic processes operating in the ionosphere since May 2018 (Guo et al., 2019, 2020; Luo et al., 2020; Chernogor et al., 2021, 2022).

The receiver system is comprised of the active antenna operating in the 10 kHz – 30 MHz frequency range, the USRP N210 software defined radio using the LFRX/LRTX daughterboards, and the personal computer, for which a sophisticated software package has been developed.

This study makes use of signals that were transmitted by the broadcasting stations at Lintong/Pucheng, Hailar/Nanmen, Beijing, Shijiazhuang, and Hohhot (PRC), Hwaseong and Goyang (Republic of Korea), Chiba/Nagara and Yamata (Japan), Ulaanbaatar/Khonkhor (Mongolia), and Yakutsk (Russian Federation), 14 propagation paths altogether, which specifications are presented in Table 2. The orientation of the propagation paths in Figure 2 shows that the propagation path midpoints were in the ionospheric regions with different Moon's coverage of the Sun. The radio system is described in more detail by Guo et al. (2019, 2020), Luo et al. (2020), and Chernogor et al. (2020, 2021).

4 Signal processing techniques

The information on ionospheric processes has been inferred from analysis of the temporal dependences of the Doppler spectra and the relative amplitudes of the radio waves received from all propagation paths. The spectrum content was determined over time intervals of 20.48 s by employing the autoregressive spectrum analysis of Marple (1987), which yields a Doppler resolution of 0.01 Hz and a temporal resolution of 7.5 s. The information is derived from temporal variations in the Doppler shift, $f_D(t)$, in the main ray, from the relative amplitudes, $A(t)$, of the signals, and from Doppler spectrum broadening. Further, the Doppler shifts, $f_D(t)$, are plotted vs. time for the main ray. Next, the $f_D(t)$ time series are processed in order to determine long-term trends, short-term fluctuations, spectral content, etc.

5 Background information on the solar eclipse

The solar eclipse of 6 January 2019 LT was observed in Asia, viz., the PRC, Japan, the Russian Federation, the Republic of Korea, and in the North Pacific Ocean (EclipseWise.com, 2019).
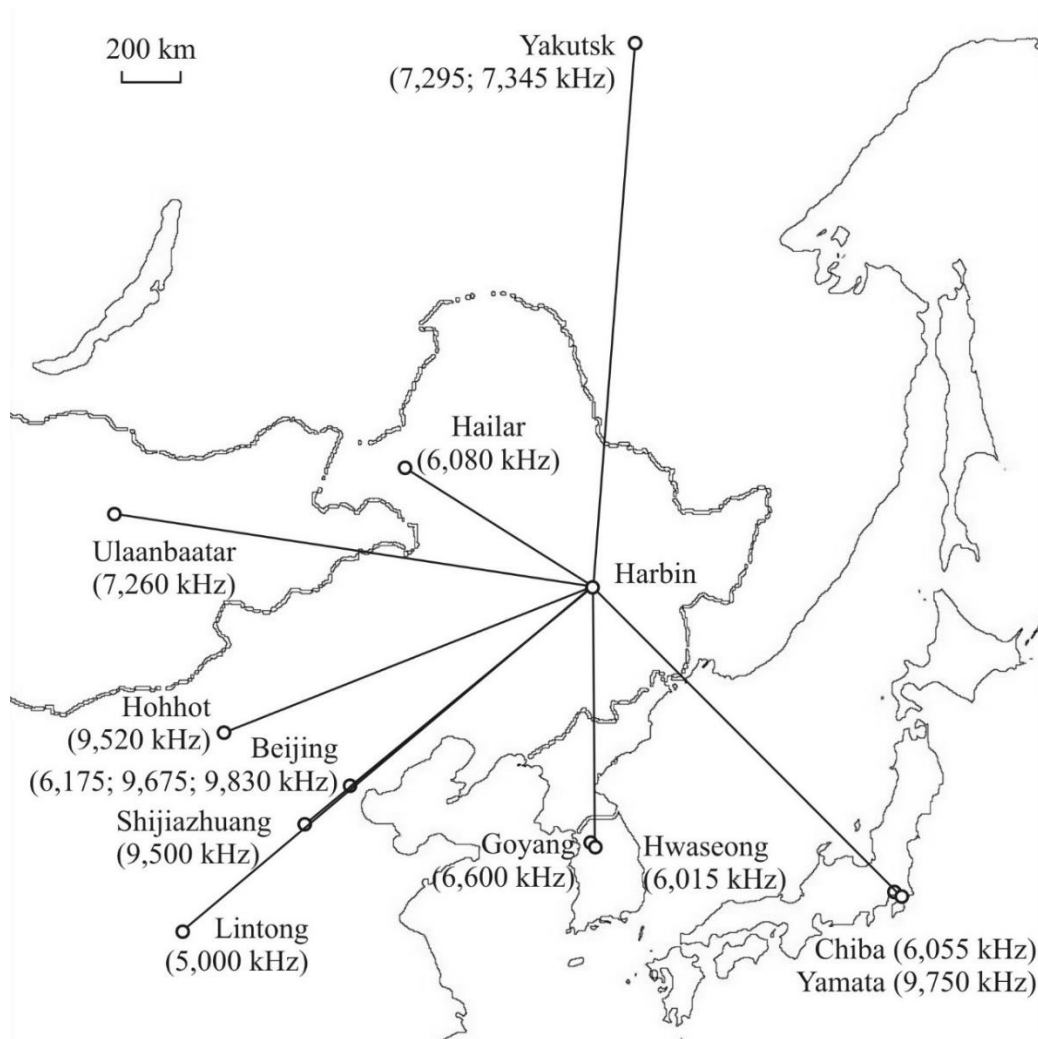
Figure 2: Schematic diagram showing the locations of the transmitters and the receiver (Harbin) connected by the great-circle propagation paths, which were used for the observation of solar eclipse effects.

In the PRC, the solar eclipse was observed to be partial (Figure 3). The eclipse magnitude, M, at an altitude of 100 km under the propagation path midpoints varied from 0.356 to 0.614, whereas the eclipse obscuration varied from 23.5 % to 51.6 % (see Table 3 where a time followed by "(r)" means the event is already in progress at sunrise). The eclipse duration changed from 133 min to 160 min. In a number of regions of the PRC, the solar eclipse began to occur before sunrise. The vertical lines in the middle panels in Figures 4–10 presenting the experimental data indicate the onset, the instant of the greatest eclipse, and the end of the solar eclipse. Generally, the effects of the solar eclipse in the ionosphere were observed to occur in the local time morning with the transient processes acting in the background.

Table 2. Basic parameters of radio paths. Retrieved from https://fmscan.org/index.php.

| Transmitter | | | | Propagation path midpoints |
Frequency (kHz)	North latitude [deg.] East longitude [deg.]	Location (country)	Distance to Harbin (km)	North latitude [deg.] East longitude [deg.]
5,000	34.95 109.56	Lintong/ Pucheng (China)	1,875	40.37 118.12
6,015	37.21 126.78	Hwaseong (Korea)	950	41.50 126.73
6,055	35.47 140.21	Chiba/ Nagara (Japan)	1,610	40.63 133.45
6,080	49.18 119.72	Hailar/ Nanmen (China)	645	47.48 123.2
6,175	39.75 116.81	Beijing (China)	1,050	42.77 121.75
6,600	37.60 126.85	Goyang (Korea)	910	41.69 126.77
7,260	47.80 107.17	Ulaanbaatar/ Khonkhor (Mongolia)	1,496	46.79 116.93
7,295	62.24 129.81	Yakutsk (Russia)	1,845	54.01 128.25
7,345	62.24 129.81	Yakutsk (Russia)	1,845	54.01 128.25
9,500	38.47 114.13	Shijiazhuang (China)	1,310	42.13 120.41
9,520	40.72 111.55	Hohhot (China)	1,340	43.25 119.12
9,675	39.75 116.81	Beijing (China)	1,050	42.77 121.75
9,750	36.17 139.82	Yamata (Japan)	1,570	40.98 133.25
9,830	39.75 116.81	Beijing (China)	1,050	42.77 121.75

6 Measurements and analysis

The 4/5 and 6/7 January 2019 UT periods have been used as reference for selecting the ionospheric perturbations caused by the solar eclipse. It should be noted that the ionosphere on 4 and 5 January 2019 was partially disturbed because the recovery phase of the moderate magnetic storm proceeded during the latter days.

The measurements were made along 14 propagation paths; however, the modes of operation of only seven transmitters provided the measurements suitable for further processing. Consider the observations and analysis in more detail.
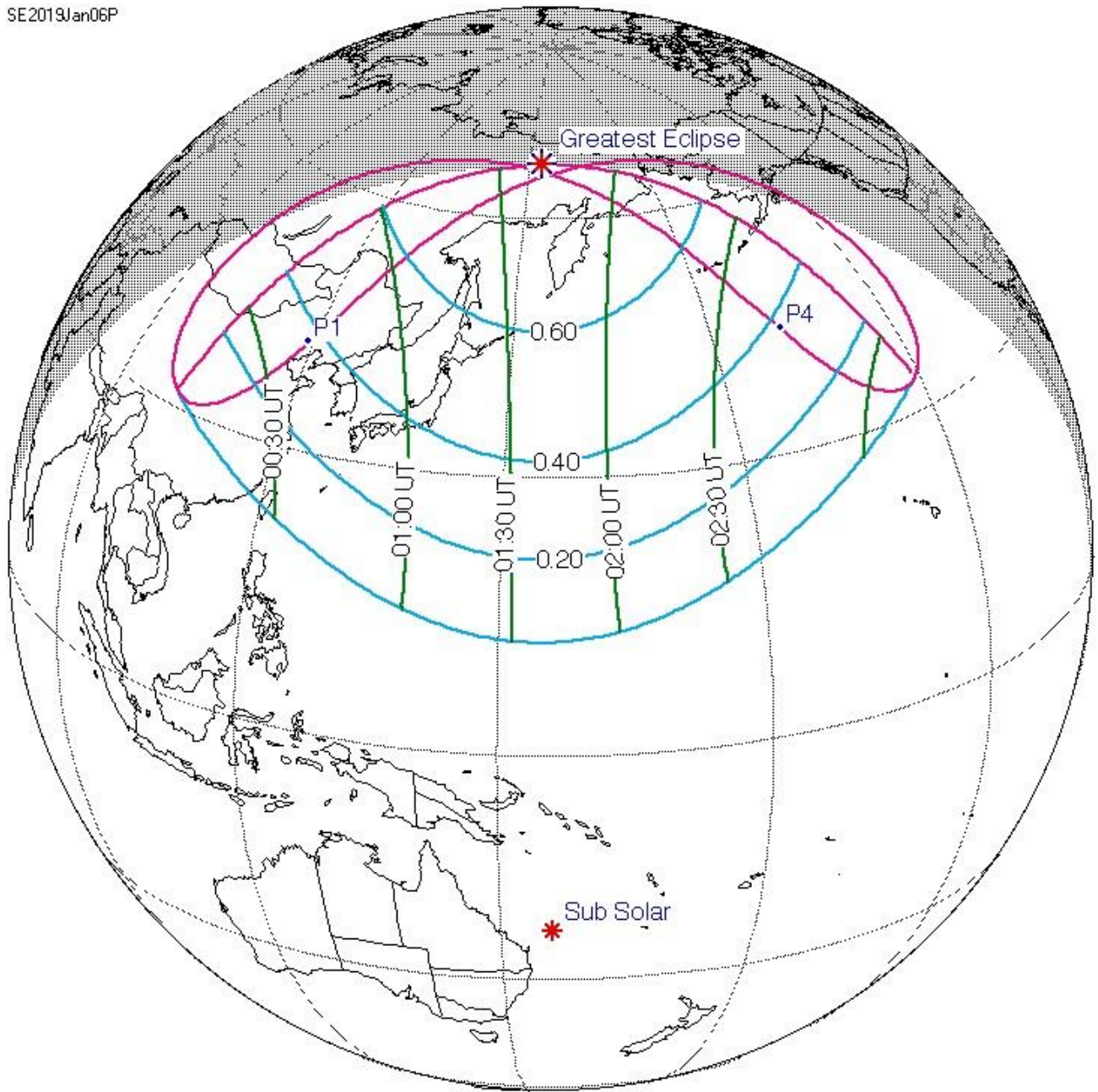
Figure 3: Schematic display of the Moon's shadow during the course of the partial solar eclipse of 5–6 January 2019. Retrieved from https://eclipse.gsfc.nasa.gov/SEplot/SEplot2001/SE2019Jan06P.GIF .

Table 3. Basic information on the solar eclipse parameters at 100 km altitude over the propagation path midpoints. Retrieved from https://eclipse.gsfc.nasa.gov/JSEX/JSEX-AS.html.

Propagation Path	Eclipse Magnitude	Eclipse Obscuration	First Contact (UT)	Sun Altitude (deg.)	Moment of Obscuration Maximum (UT)	Sun Altitude (deg.)	Sun Azimuth (deg.)	Fourth Contact (UT)	Sun Altitude (deg.)
Lintong/ Pucheng to Harbin	0.356	0.235	23:33(r)	0(r)	00:35:08	09	130	01:46:28	18
Hwaseong to Harbin	0.448	0.326	23:32:46	04	00:46:40	15	139	02:09:54	23
Chiba/ Nagara to Harbin	0.483	0.362	23:35:58	09	00:56:19	19	147	02:26:14	26
Hailar/ Nanmen to Harbin	0.514	0.395	23:37(r)	0(r)	00:48:36	09	138	02:11:06	16
Beijing to Harbin	0.43	0.307	23:31:51	00	00:41:37	11	135	02:00:00	19
Goyang to Harbin	0.451	0.329	23:32:49	04	00:46:54	14	140	02:10:18	23
Ulaanbaatar/ Khonkhor to Harbin	0.457	0.335	00:00(r)	0(r)	00:41:14	05	131	01:57:18	14
Yakutsk to Harbin	0.624	0.516	23:49(r)	0(r)	01:02:22	07	145	02:28:34	12
Yakutsk to Harbin	0.624	0.516	23:49(r)	0(r)	01:02:22	07	145	02:28:34	12
Shijiazhuang to Harbin	0.408	0.285	23:31:34	00	00:39:25	10	133	01:55:39	19
Hohhot to Harbin	0.416	0.293	23:38(r)	0(r)	00:39:14	08	132	01:54:58	17
Beijing to Harbin	0.43	0.307	23:31:51	00	00:41:37	11	135	02:00:00	19
Yamata to Harbin	0.487	0.367	23:35:56	09	00:56:15	19	147	02:26:07	26
Beijing to Harbin	0.43	0.307	23:31:51	00	00:41:37	11	135	02:00:00	19

6.1 Lintong/Pucheng to Harbin radio-wave propagation path

220   This radio station, operating at 5,000 kHz, is located in the PRC at a great-circle distance, R, of 1,875 km from Harbin. The eclipse magnitude, M_{max}, at an altitude of 100 km under the propagation path midpoint was estimated to be 0.356, whereas the eclipse obscuration, B_m, was predicted to be 0.235.

Figure 4 shows UT dependences of the Doppler spectra exhibiting diffuseness and occupying the frequency range from zero to 1.5 – 2.5 Hz were observed in the local time morning on both the reference days and the day when the solar

225   eclipse occurred. On 5 January 2019, the Doppler shift in the main (maximum energy) ray first increased, fluctuating, from zero to 0.6 Hz at 00:30 UT, and then decreased to zero. The Doppler shift exhibited ~4 – 5 min period, T, and 0.1 Hz

amplitude, f_{Da}, quasi-periodic variations over the 00:50 – 01:45 UT period. The Doppler spectra showed that virtually one ray was reflected from the ionosphere over the 01:00–03:00 UT period.
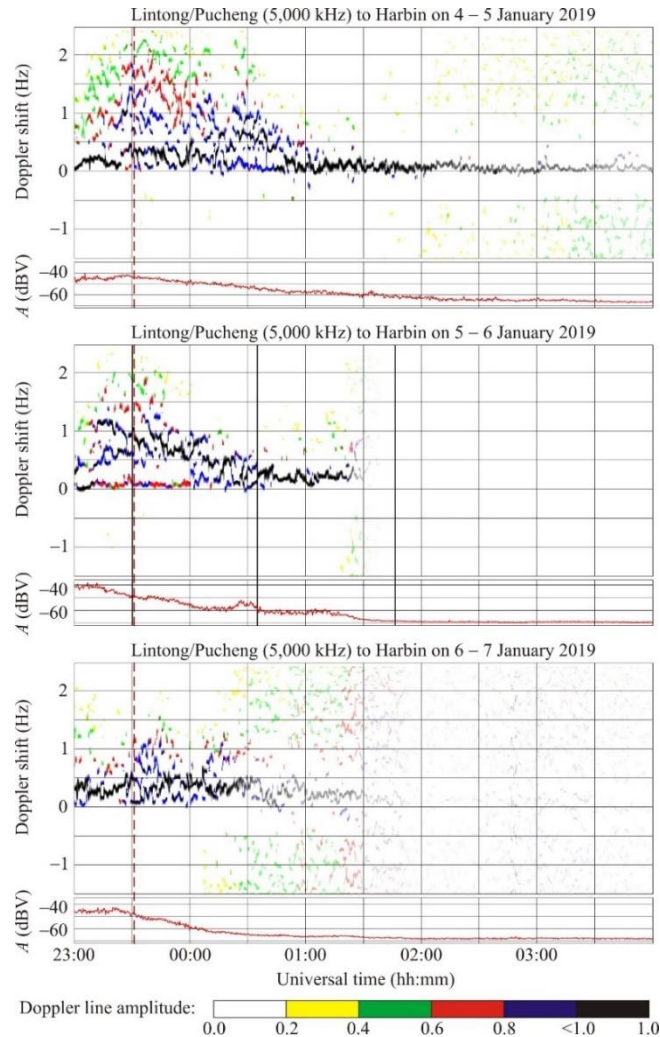
230

Figure 4: Universal time variations of Doppler spectra and signal amplitude, *A*, along the Lintong/Pucheng to Harbin propagation path. The black-blue-red-green-yellow colors show the relative amplitude of 1, 0.8, 0.6, 0.4, and 0.2, respectively. The vertical solid lines indicate, hereafter, the beginning, maximum phase, and the end of the solar eclipse at 100 km altitude, whereas dashed lines indicate sunrise at ground level because the sunrise at 100 km altitude occurred beyond the UT axis range, i.e., before 23:00 UT.

235

On 7 January 2019, the Doppler spectrum broadening did not exceed 1.5 Hz until 00:30 UT, and diffuseness exhibited an increase over the 00:30 – 02:00 UT period. The Doppler shift in the main ray exhibited variations from 0.3 Hz to 0.5 Hz, with a quasi-period, *T*, of ~25 min and amplitude, f_{Da}, of 0.1 Hz.

On 5 January 2019, during the 23:00 – 23:45 UT period, the Doppler spectrum broadening attained 2 Hz, whereas during the time interval from 23:45 UT on 5 January 2019 to 00:15 UT on 6 January 2019, it did not exceed 1 Hz. After this time interval, the Doppler spectra showed that one ray was reflected from the ionosphere until 01:30 UT on 6 January 2019.

Before the solar eclipse onset, i.e., before approximately 23:30 UT on 5 January 2019, the mean, $\overline{f_D}$, of the Doppler shift in the main ray was observed to be approximately 1.2 Hz. Over the time interval from 23:30 UT on 5 January 2019 to 00:35 UT on 6 January 2019, the mean, $\overline{f_D}$, showed a tendency to decrease from 1 Hz to 0.1 Hz, whereas $\overline{f_D} \approx 0.1 - 0.2$ Hz to the end of the eclipse. The spectrum of fluctuations in $f_D(t)$ showed oscillations with a period, T, of ~10 – 15 min and amplitude, f_{Da}, of 0.1 Hz.

On the reference days, the signal amplitude, A, exhibited monotonous changes, viz., the amplitude decreased by 25 dBV as the ionosphere went out of and into sunlight. On 6 January 2019, from 00:22 UT until 00:37 UT, i.e., around the maximum phase of the eclipse, the signal amplitude first showed an increase by 7 dBV and then a decrease close to the previous value.

6.2 Chiba/Nagara to Harbin radio-wave propagation path

This radio station, operating at 6,055 kHz, is situated in Japan at a great-circle distance, R, of ~1,610 km from Harbin. At the middle of the propagation path, $M_{max} \approx 0.483$, $B_m \approx 0.362$.

During the 4/5 January 2019 UT night, from 23:00 to 01:30 UT, the Doppler spectra exhibited diffuseness (Figure 5), whereas the spectrum width attained 1.3 Hz. During the 01:30–03:40 UT period, the Doppler spectra showed that a single ray was reflected from the ionosphere, and the Doppler shift in the main ray exhibited variations from zero to 0.6 Hz. During the 6/7 January 2019 UT reference period, the Doppler spectra showed the following behavior. From 23:00 UT to 01:30 UT, the Doppler spectrum diffuseness was observed to occur, whereas spectrum broadening attained 1 Hz, and the spectra showed that virtually a single ray was reflected from the ionosphere after 01:30 UT. The ~5 – 7 min period, T, and ~0.10 – 0.15 Hz amplitude, f_{Da}, oscillations were observed to occur in the spectrum of $f_D(t)$ in the main ray.

During the 5/6 January 2019 night, from 23:00 UT to 01:50 UT, the Doppler spectra showed diffuseness, whereas the f_D values exhibited high temporal variability from –(1 – 1.5) Hz to (1 – 1.2) Hz. After the solar eclipse onset, the Doppler spectrum width varied within the 0.5 Hz limits. From 01:00 UT, it again occupied the range from –1.5 Hz to 1.2 Hz, whereas the Doppler shift temporal dependence in the main ray showed gaps. The $\overline{f_D}$ showed a tendency to decrease from 0.5 Hz to – 0.3 Hz within the 23:00 UT to 00:30 UT interval, then it was fluctuating around zero over the 00:30 – 01:00 UT period, after which the $\overline{f_D}$ exhibited a tendency to increase from 0 Hz to 0.6 Hz over a half hour interval, i.e., until 01:30 UT. Around the maximum phase of the eclipse, the ~10 min period, T, and ~0.10 – 0.15 Hz amplitude, f_{Da}, oscillations were observed to occur, while the signal amplitude exhibited an increase up to 5 dBV over about a 20 min interval. Similar effects were absent on the reference days.

13
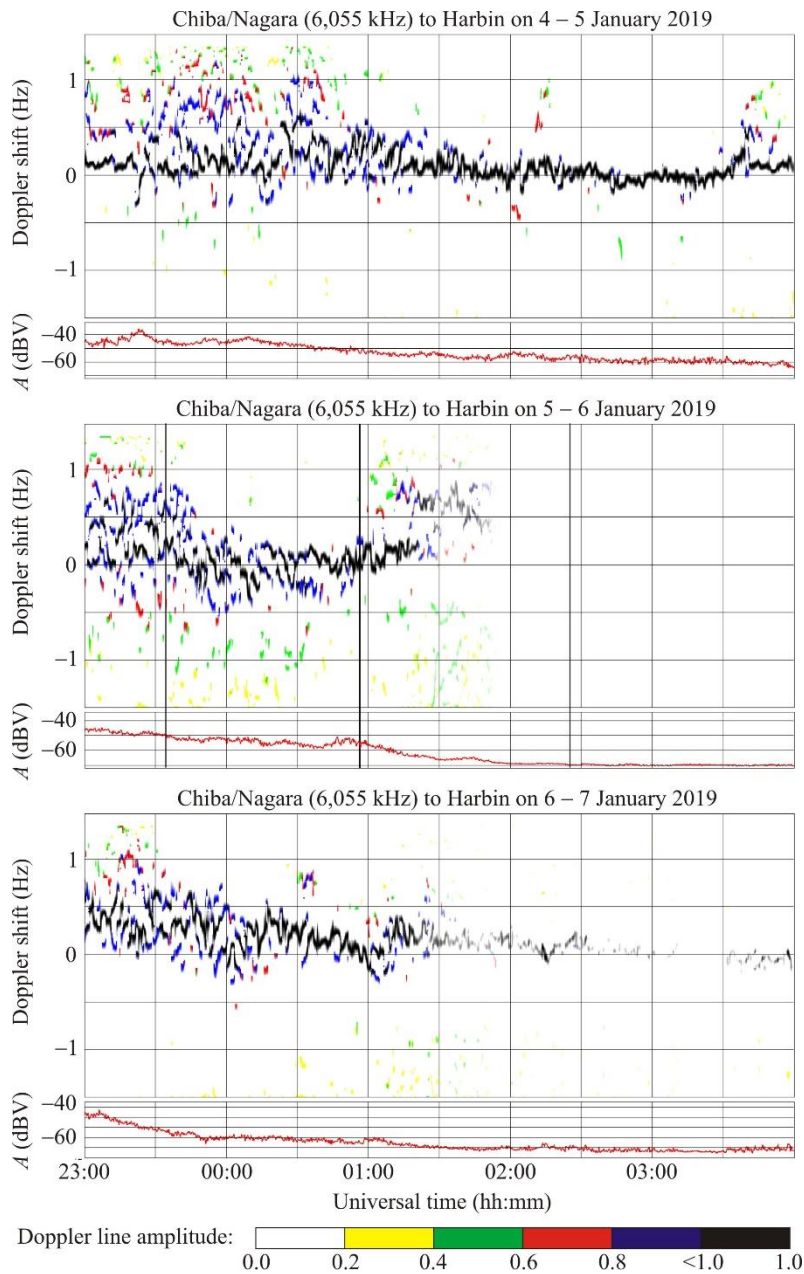
Figure 5: The same as in Figure 4 but for the Chiba/Nagara to Harbin radio-wave propagation path.

6.3 Ulaanbaatar to Harbin radio-wave propagation path

This radio station, operating at 7,260 kHz, is located in Mongolia at a great-circle range, R, of ~1,496 km from Harbin. The solar eclipse magnitude, M_{max}, at an altitude of 100 km under the midpoint of this propagation path is estimated to be ~0.457, whereas the eclipse obscuration, B_m, is predicted to be ~0.335.

14

During the 4/5 January 2019 night, from 23:00 to 01:00 UT, and from 01:50 to 02:50 UT, the Doppler spectra exhibited considerable broadening, from –1.5 Hz to 1.5 Hz (see Figure 6). The Doppler shift in the main ray showed a decrease, time fluctuating, from 1 Hz observed at the end of 4 January 2019 to zero on 5 January 2019, whereas the range of fluctuations attained 0.20 – 0.25 Hz.

280   Consider the behavior of the Doppler spectra during the transition from 6 to 7 January 2019. On 6 January 2019, from about 23:20 UT to 24:00 UT, the spectra showed diffuseness and occupied the band of frequency from –(1 – 1.5) Hz to 1.5 Hz, while the main ray showed fluctuations around the –1 Hz level. On 7 January 2019, after 00:00 UT, a sharp increase in the Doppler shift took place from –1 Hz to 0.5 Hz, and then a decrease in $f_D(t)$ was noted from 0.5 Hz to 0 Hz, while the $f_D(t)$ exhibited fluctuations within the 0.2 Hz limits.

285   The Doppler spectra showed broadening before the solar eclipse onset, whereas the range of fluctuations in $f_D(t)$ was observed to be close to 0.2 Hz. The transmitter was out of operation over the 00:05 – 00:50 UT period on 6 January 2019; after 00:50 UT, the Doppler spectra showed that virtually a single ray was reflected from the ionosphere, and the $f_D(t)$ showed a tendency, first, to increase to 01:15 UT, and then to decrease from 0.8 Hz to 0.2 Hz at 03:00 UT.

During all days, the signal amplitude exhibited fluctuations within the 10 dBV limits. Effects of the solar eclipse
290   were not observed reliably in the signal amplitude.

6.4 Shijiazhuang to Harbin radio-wave propagation path

This transmitter, operating at 9,500 kHz, is situated in the PRC at a great-circle range, R, of ~1,310 km from the receiver at Harbin. The solar eclipse magnitude, M_{max}, at an altitude of 100 km under the midpoint of this propagation path is estimated to be ~0.408, whereas the eclipse obscuration, B_m, is predicted to be ~0.285.

295   During the 4/5 January 2019 night, from 23:20 to 00:30 UT, the Doppler spectra were observed to broaden, from 0 Hz to 1.5 Hz (see Figure 7), whereas from 23:40 to 01:00 UT, the Doppler shift in the main ray showed a decrease from 0.25 Hz to 0 Hz. During the 6/7 January 2019 night, from 23:30 to 04:00 UT, the Doppler spectra showed that a single ray was reflected from the ionosphere, while the $f_D(t)$ exhibited a decrease, fluctuating, from 0.3 Hz to 0.1 Hz.

On the local time day, when the solar eclipse occurred, the Doppler spectra and the Doppler shifts were notably
300   different from those observed on the reference days. On the night of 5/6 January 2019, until 23:30 UT, the fluctuations in $f_D(t)$ were insignificant since the radio waves were reflected from the sporadic E layer, whereas from 23:30 UT to 01:00 UT the radio waves were reflected from the F region, and consequently the $f_D(t)$ were observed to fluctuate widely, from 0.4 Hz to –0.2 Hz. The $\overline{f_D}(t)$ showed a tendency to decrease quasi-periodically from 0.4 Hz to 0.2 Hz over the 23:30 – 24:00 UT period, with the ~10 – 15 min period, T, and ~0.1 Hz amplitude, f_{Da}, variations being superimposed on the $\overline{f_D}(t)$.
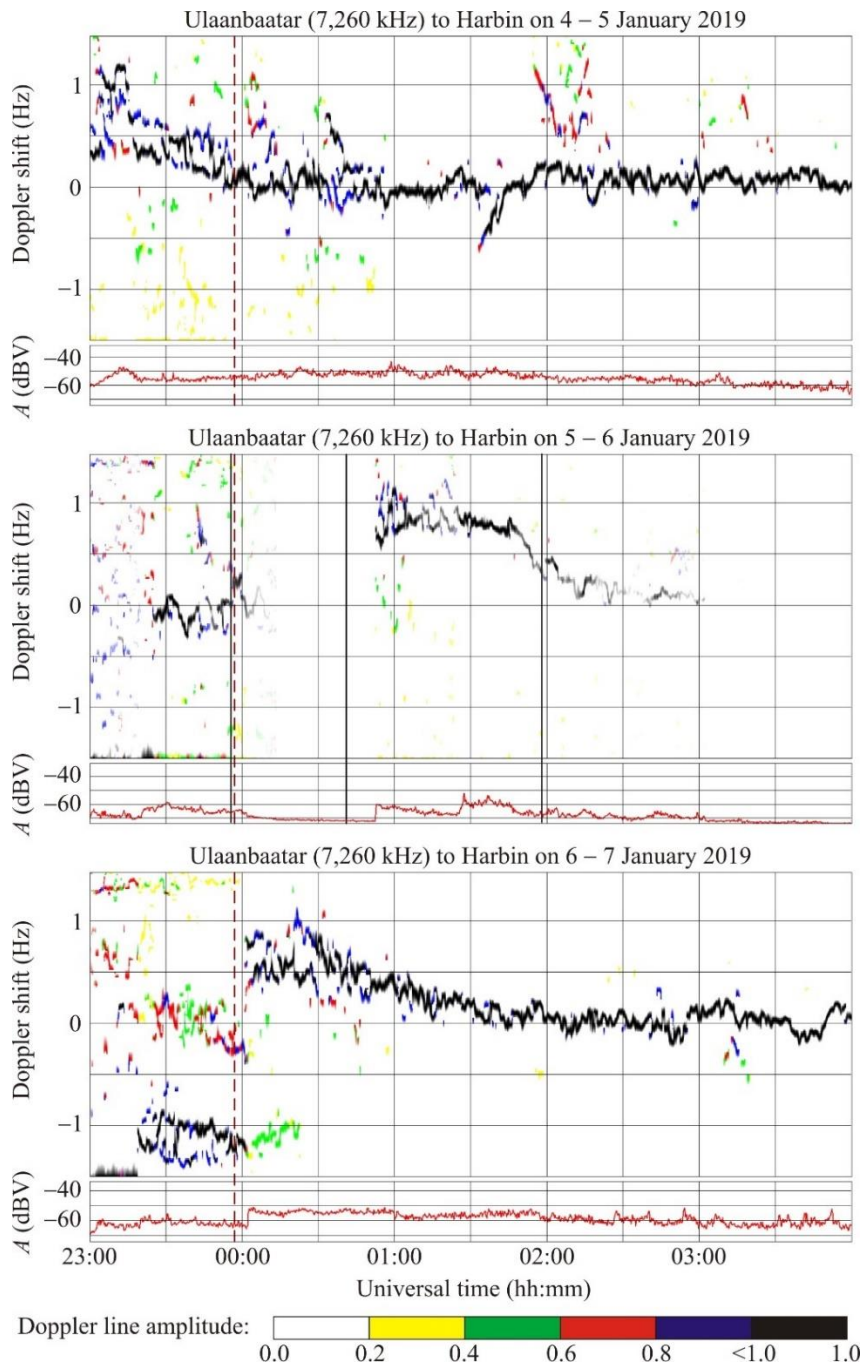
Figure 6: The same as in Figure 4 but for the Ulaanbaatar to Harbin radio-wave propagation path.
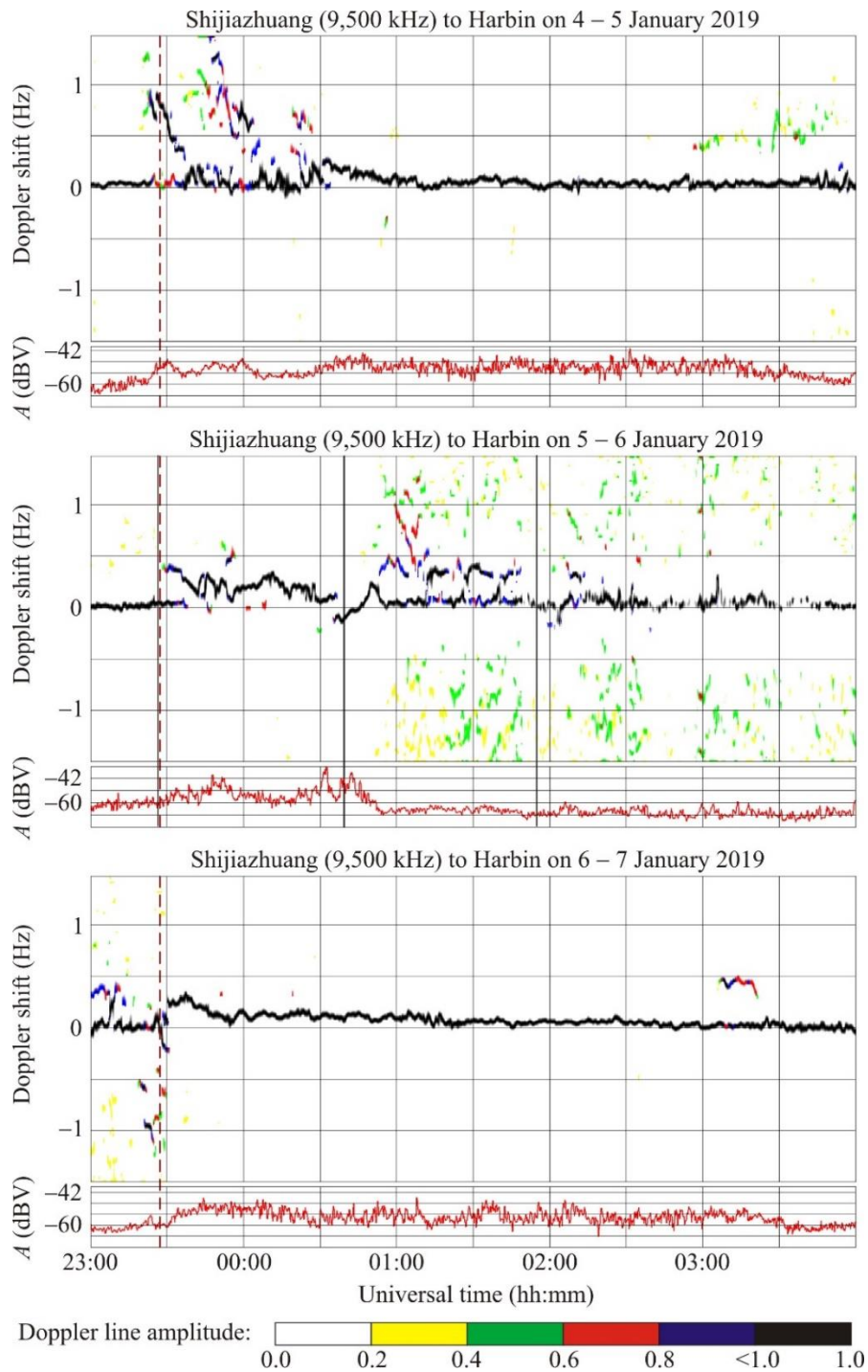
305

16

Figure 7: The same as in Figure 4 but for the Shijiazhuang to Harbin radio-wave propagation path.

310   On 6 January 2019, from 00:00 UT and to 00:30 UT, $\overline{f_D}(t) \approx 0.2$ Hz. Around the instant of the greatest occultation of the Sun's area, $\overline{f_D} \approx 0$ Hz, after which the $\overline{f_D}$ was observed to grow from nearly zero to 0.25 Hz in 15 min, and then the $\overline{f_D}$ exhibited a decrease from 0.25 Hz to zero. A partial screening of reflections from the F layer by the sporadic E layer was noted after about 00:55 UT on 6 January 2019, whereas a significant (from –1.5 Hz to 1.5 Hz) broadening appeared in the Doppler spectra. Two Doppler lines, with $\overline{f_D}(t) \approx 0.1$ Hz and $\overline{f_D}(t) \approx 0.4$ Hz, were the more conspicuous in the Doppler

315   spectrum within the 00:50 – 01:45 UT period on 6 January 2019.

        The signal strengths exhibited high temporal variability (up to 12 dBV) along this propagation path during the reference days, whereas during the 5/6 January 2019 night, from 23:35 to 00:40 UT, i.e., around the instant of greatest eclipse, variations in $A(t)$ attained 18 dBV.

6.5 Hohhot to Harbin radio-wave propagation path

320   This propagation path at ~9,520 kHz passes in the PRC over the great-circle path length, R, of ~1,340 km. At the transmitter location, $M_{max} \approx 0.416$, $B_m \approx 0.293$.

        In the course of the 4/5 January 2019 night, the Doppler spectra showed that a single ray was reflected almost all the time from 23:40 UT to 04:00 UT (Figure 8). The spectrum broadening from 0.5 Hz to 1.5 Hz was observed to occur only over the 23:20 – 23:55 UT period. The Doppler spectra showed that two rays were reflected from the ionosphere over the

325   02:45 UT to 03:50 UT period, whereas the $f_D(t)$ was observed to exhibit high temporal variability from 00:00 to 01:00 UT. During the 6/7 January 2019 night, the Doppler spectra showed that only a single ray was reflected from the ionosphere virtually all the time from 23:00 to 04:00 UT, whereas the $f_D(t)$ exhibited high temporal variability over the 23:40 – 01:00 UT period.

        The equality $\overline{f_D}(t) \approx 0$ Hz was observed to hold during the 5/6 January 2019 night before the solar eclipse, when

330   the radio wave began reflecting from the ionospheric F region. The Doppler shift exhibited a decrease from 0.5 Hz to 0.1 Hz during the following 30 min, and during the time interval until 00:30 UT, the $\overline{f_D}(t)$ showed a decrease from 0.1 Hz to 0 Hz. The $f_D(t)$ exhibited high (from 0.5 Hz to 0 Hz) temporal variability over the 00:30 – 02:30 UT period, after which the range of fluctuations did not exceed 0.2 Hz. The ~15 min period, T, and ~0.10 – 0.15 Hz amplitude, f_{Da}, Doppler lines were noted during the solar eclipse.

335   During the 23:40–00:25 UT period in the course of the solar eclipse on 5/6 January 2019 night, the signal amplitude exhibited an increase by 20 – 25 dBV, whereas the increase shown by A on the reference days did not exceed 10 – 15 dBV.
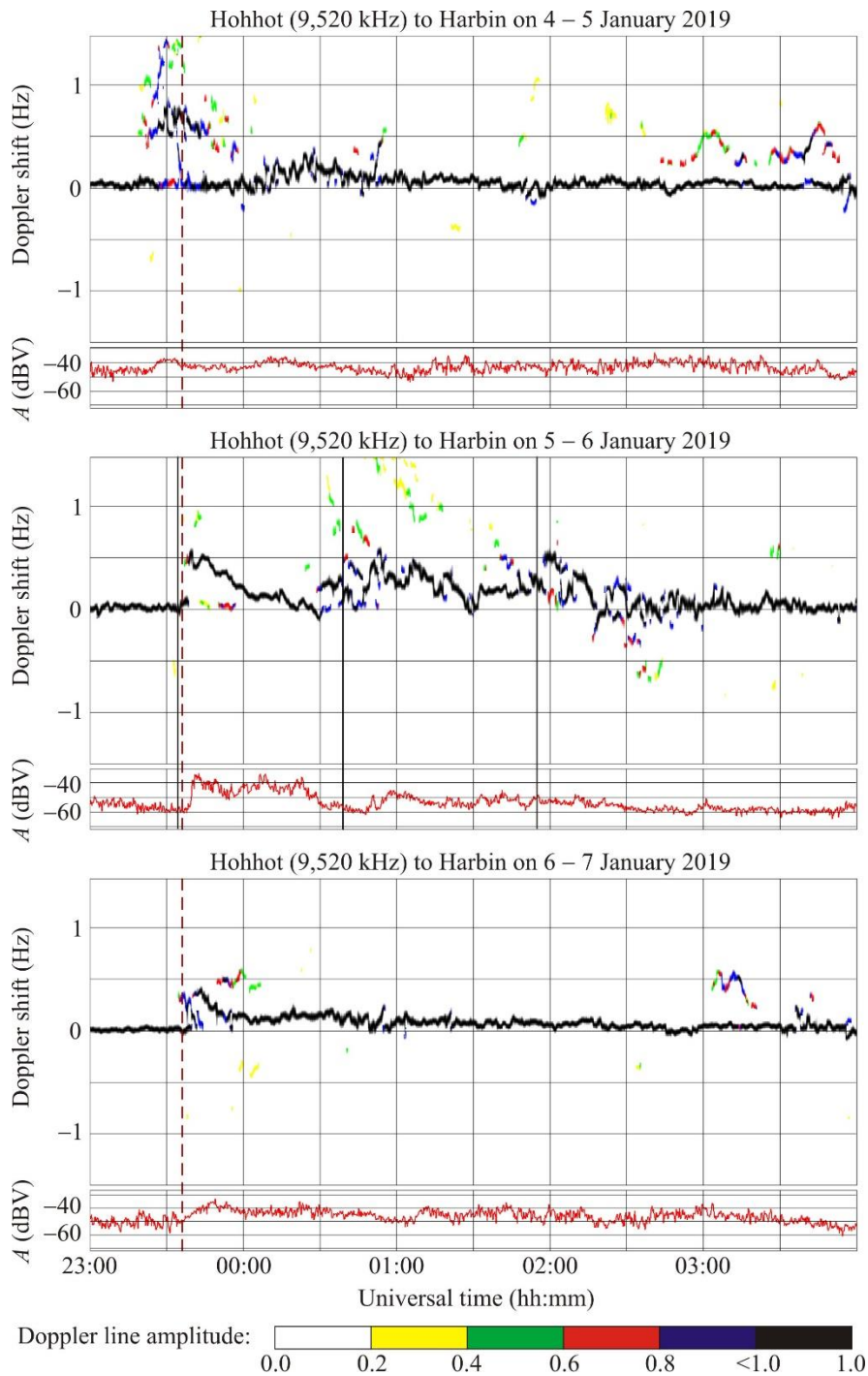
Figure 8: The same as in Figure 4 but for the Hohhot to Harbin radio-wave propagation path.

6.6 Beijing to Harbin radio-wave propagation path

This radio station operating at 9,675 kHz is located in the PRC at a great-circle range, R, of ~1,050 km from the receiver at Harbin. The solar eclipse magnitude M_{max} at the location of the transmitter is estimated to be ~0.430, whereas the eclipse obscuration, B_m, to be ~0.307.

Figure 9 shows that the Doppler shift trend $\overline{f_D}(t) \approx 0$ until 00:30 UT on the 4/5 January 2019 night. The Doppler shift exhibits quasi-periodic variations with an ~20 min period, T, and an ~0.15 Hz amplitude, f_{Da}, over the 00:30 – 02:00 UT period. The Doppler spectra show that single rays are reflected from the ionosphere almost all the time, whereas the Doppler spectra exhibited broadening only during the 23:35 UT and 00:25 UT periods. During the 6/7 January 2019 night, the Doppler spectra showed that single rays were reflected from the ionosphere. The $f_D(t)$ exhibited quasi-periodic variations with an amplitude of about 0.1 Hz and a period changing from 15 min to 20 min over the 23:45–01:45 UT period.

Consider the time interval around the solar eclipse on the 5/6 January 2019 night. The trend $\overline{f_D}(t) \approx 0$ until 23:50 UT. Then it showed an increase from zero to 0.4 Hz, which was followed by a decrease to zero, over the 23:50–00:20 UT period. The ~4 – 5 min period, T, and ~0.05 Hz amplitude quasi-periodic variations were noted in $f_D(t)$ over the 00:42–02:15 UT period. In addition, other Doppler lines 0.5 – 1 Hz apart from the main line were observed to occur over the 00:55 – 03:00 UT period.

The signal amplitude showed variability within the 3–5 dBV limits on the reference days, whereas it exhibited an increase to 10 – 20 dBV in the course of the solar eclipse.

6.7 Beijing to Harbin radio-wave propagation path

This radio station, broadcasting at 9,830 kHz, occupies the same site as the radio station broadcasting at 9,675 kHz; since the operating frequencies are close to each other, all effects observed at these two frequencies are similar, as can be seen in Figure 10.
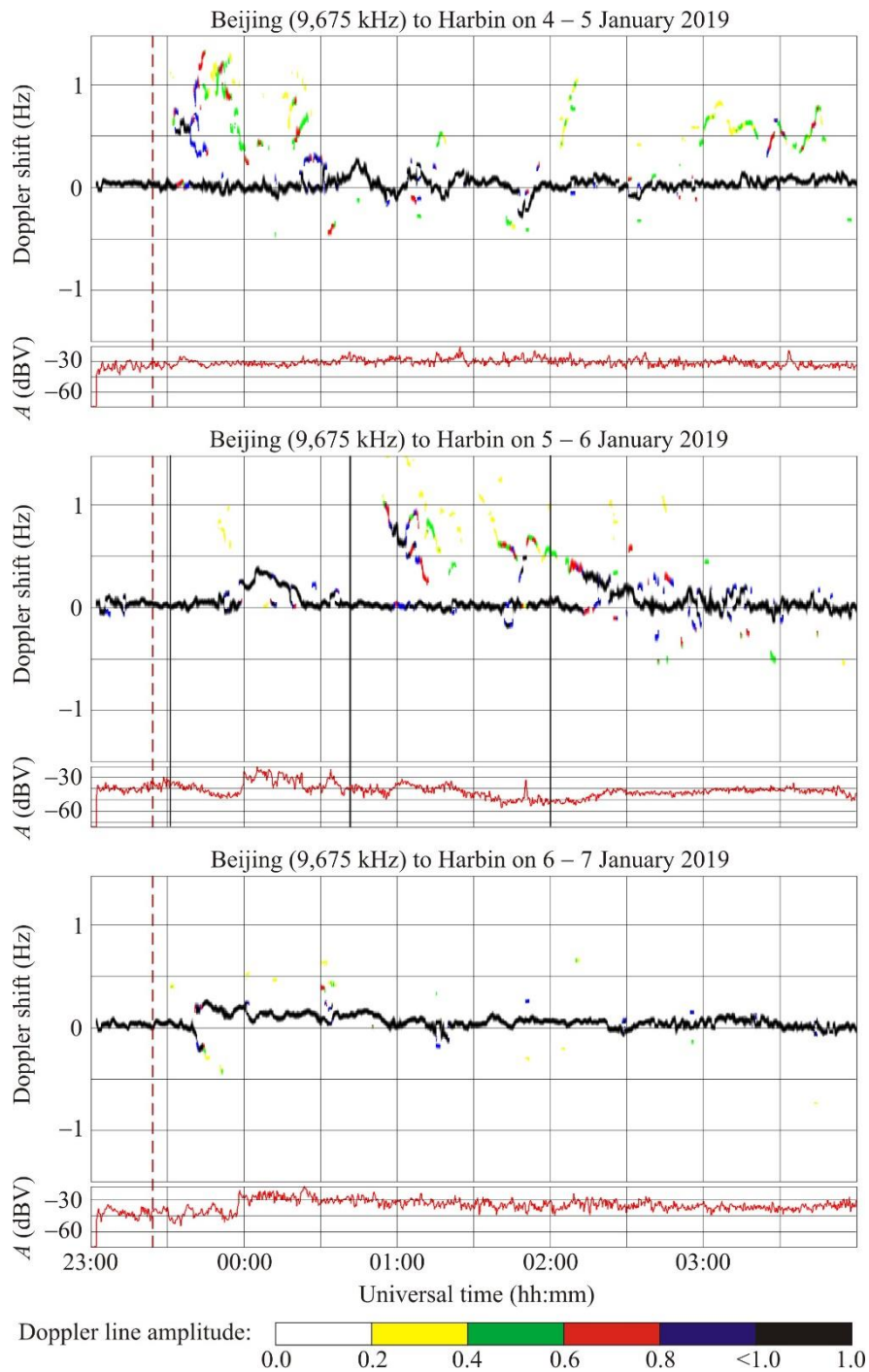
Figure 9: The same as in Figure 4 but for the Beijing to Harbin radio-wave propagation path.
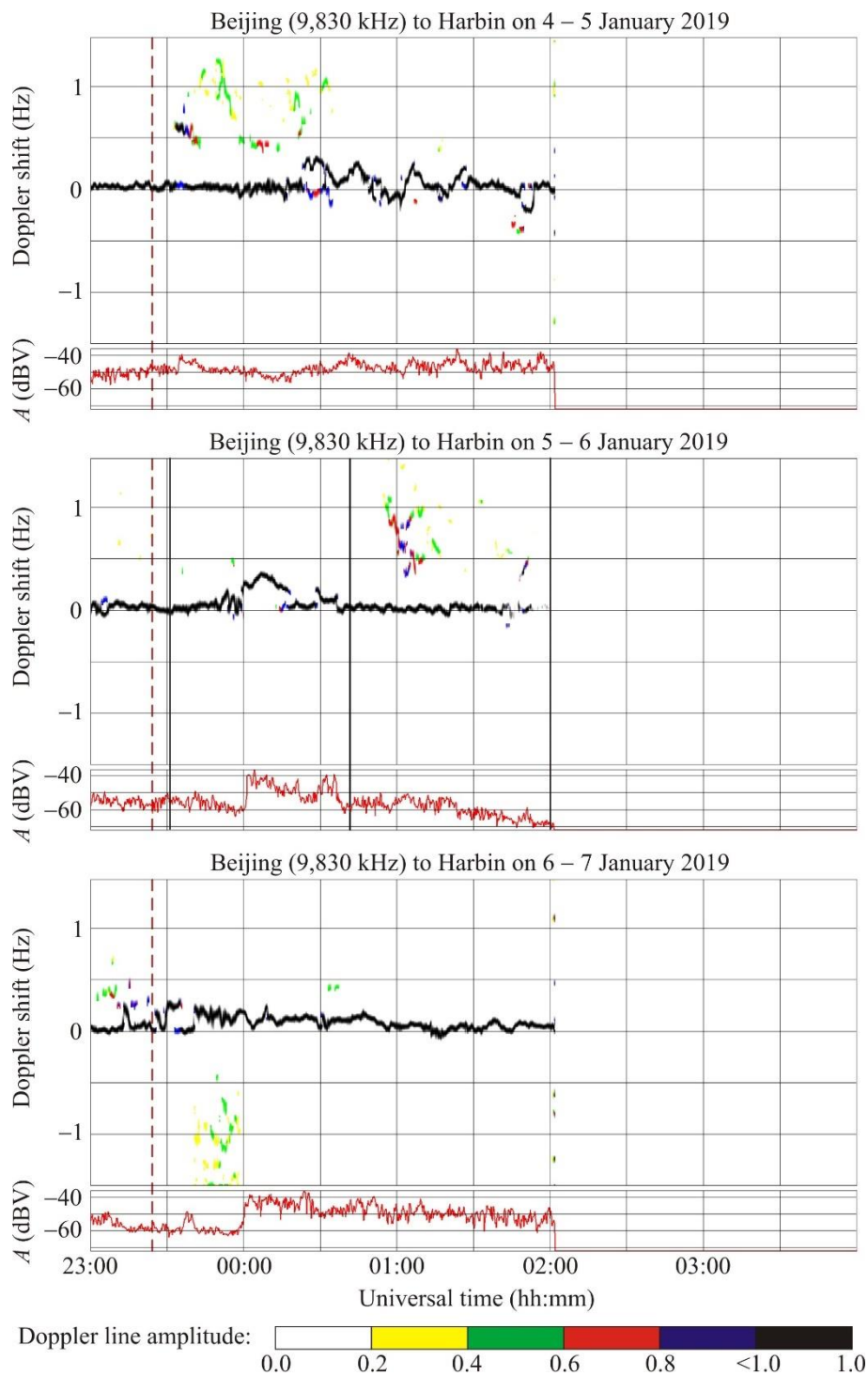
365

Figure 10: The same as in Figure 4 but for the Beijing to Harbin radio-wave propagation path.

22

7 Discussion

7.1 Effects from solar eclipses

Solar eclipses are well known for having the capability to cause significant variations in the parameters of both the medium and the geophysical fields in all subsystems in the Earth–atmosphere–ionosphere–magnetosphere system (see, e.g., Chernogor, 2003, 2011, 2013a; Chernogor and Rozumenko, 2008). Solar eclipses act to notably cool the air and the ground surface, to decrease the air pressure, etc. The plasma parameters and dynamics in the ionosphere show significant changes: the electron density decreases, the ion and electron temperatures reduce, the rates of chemical reactions alter, the settled coupling between the ionosphere and the plasmasphere becomes disturbed, the precipitation of energetic electrons is made possible from the magnetosphere into the atmosphere causing additional ionization (Chernogor, 2013a). Özcan and Aydoğdu (2004) and Chernogor (2012, 2013a) also describe the effects of solar eclipses in the geomagnetic field.

The regular effects of solar eclipses may be regarded as quite well known, whereas irregular effects and their influence on the propagation of radio waves in various frequency bands have been studied to a lesser degree. On the one hand, the irregular effects in the Earth–atmosphere–ionosphere–magnetosphere system are associated with the generation of different kinds of instability in the atmosphere and in its ionized components, turbulence production in these media, the amplification and generation of the waves of various nature (infrasound, atmospheric gravity waves, magnetohydrodynamic waves, etc.) On the other hand, the irregular effects significantly depend on the subsystem perturbation in the Earth–atmosphere–ionosphere–magnetosphere system, on the state of atmospheric and space weather, season, local time, the phase of the solar eclipse, and on the geographic coordinates of the observation site. The scientific studies conducted for many years have shown that the responses of the subsystems in the Earth–atmosphere–ionosphere–magnetosphere system to the solar eclipses that occurred over the period from the end of the twentieth century to the beginning of the twenty-first century have never been the same (Chernogor, 2013a).

7.2 Basics of the variations in the Doppler shift during solar eclipses

It is known that for a plane stratified isotropic ionosphere the Doppler shift is given by (see, e.g., Davies, 1990)

$$f_D = -\frac{f}{c}\frac{d}{dt}\int_s n\,ds = -2\frac{f}{c}\int_0^{z_r} n\sec\vartheta\,dz \qquad (1)$$

where f is the frequency, c is the speed of light, t is time, n is the refractive index, $ds = \sec\vartheta\,dz$ is the path element, $\vartheta(z)$ is the angle that the ray makes with the vertical, z_r is the altitude of reflection.

Taking into account the dependence

$$n = n\big(N\big(\chi(t), B(t)\big)\big),$$

in Eq. (1) yields

$$f_D = -\frac{f}{c}\int_s \frac{dn}{dN}\frac{dN}{dt}\,ds = -\frac{f}{c}\int_s \frac{dn}{dN}\left(\frac{\partial N}{\partial \chi}\frac{d\chi}{dt} + \frac{\partial N}{\partial B}\frac{dB}{dt}\right)ds \tag{2}$$

Here, N is the electron density, $\chi(t)$ is the solar zenith angle, $B = S(t)/S_0$ is eclipse obscuration, S_0 is the Sun's surface area, $S(t)$ is the Sun's surface area occulted by the Moon. Equation (2) suggests that the behavior of $f_D(t)$ depends on the rate of change of $d\chi/dt$, $\partial N/\partial B$, and dB/dt with time. It should be noted that $dn/dN < 0$ for a plasma. In addition, $\partial N/\partial \chi < 0$, $\partial N/\partial B < 0$. During the morning hours, $d\chi/dt < 0$, whereas $d\chi/dt > 0$ during the course the afternoon hours.

First, consider the classical picture of the behavior of the Doppler shift $f_D(t)$, which take place around the local noon, $d\chi/dt \approx 0$, in the absence of fluctuations in the parameters of the medium. In this case, the magnitude and sign of $f_D(t)$ is dependent only on the multiplier dB/dt.

The equality $dB/dt = 0$ holds before the solar eclipse onset ($t = t_1$), at the moment, t_m, when the coverage of the Sun's surface area by the Moon is a maximum, and after the solar eclipse ceases to exist ($t = t_2$). If $t < t_m$, $dB/dt > 0$, whereas if $t > t_m$, $dB/dt < 0$. Note that the $f_D(t)$ is a two-lobe dependence symmetrical about the moment, t_m, of maximum coverage of the Sun's surface area by the Moon. Within the first lobe $t < t_m$, $f_D(t) < 0$; and within the second one $t > t_m$, $f_D(t) > 0$. At $t = t_m$, the value of $f_D(t_m)$ vanishes. It is important that $|f_{D\min}| = f_{D\max}$.

Away from the local noon, the magnitude and sign of $f_D(t)$ is determined by the relation between the expressions $(\partial N/\partial \chi)\cdot(d\chi/dt)$ and $(\partial N/\partial B)\cdot(dB/dt)$ and by the signs of $d\chi/dt$, dB/dt. At the stage when the occultation of the solar disk is increasing, $f_D < 0$, whereas at $t = t_m$, $f_D = 0$. At the stage when the occultation of the solar disk is decreasing, $f_D > 0$. The Doppler shift, $f_D(t)$, shows a minimum, $f_{D\min}$, at the moment $t = t_{\min}$, which is found within the interval $t_1 < t_{\min} < t_m$; whereas the Doppler shift, $f_D(t)$, shows a maximum, $f_{D\max}$, at the moment $t = t_{\max}$, which is found within the interval $t_m < t_{\max} < t_2$. It is important that $|f_{D\min}| \neq f_{D\max}$.

If a solar eclipse begins during the morning hours, the first term in the integrand of Eq. (2) is positive, and its value can become equal to or greater than the value of the second term, which is negative if $t_1 < t < t_m$. As a result, the effect of suppression arises in the response of the Doppler shift to the solar eclipse when an increase in N in the morning partially or totally compensate a decrease in N due to covering the solar disk. During the $t_m < t < t_2$ interval, $dB/dt < 0$, and both the terms in the integrand of Eq. (2) are positive, and consequently an increase in the Doppler shift occurs.

If a solar eclipse begins, $t_1 < t < t_m$, during the local afternoon when $d\chi/dt > 0$, and both the terms in the integrand of Eq. (2) are negative, the Doppler shift exhibits the effect of amplification. If a solar eclipse ceases to exist, $t_m < t < t_2$, during the local afternoon, the terms in the integrand of Eq. (2) have different signs (the first one is negative, and the second one is positive), the Doppler shift shows the effect of suppression.

Thus, the real $f_D(t)$ dependence may significantly differ from the classical one. In addition, the fluctuations and quasi-periodic variations in the Doppler shift are superimposed on the aperiodic changes in the trend $\overline{f_D}(t)$.

7.3 Influence of the solar terminator on the Doppler shift

This solar eclipse took place before and immediately after the sunrise and morning period, which is one of its features. Therefore, the effects of the dawn terminator could be significant. The Doppler spectra show that the movement of the solar terminator was accompanied by significant diffuseness along virtually all propagation paths, whereas the Doppler spectra broadening attained $1.5 - 2.5$ Hz. In addition, the Doppler shift exhibited noticeable variations in the main ray. The mentioned above effects were absent along both Beijing to Harbin propagation paths. Most probably, sporadic E propagation took place along these propagation paths, along which $f_D(t) \approx 0$ Hz, and diffuseness in the Doppler spectra was absent.

The analysis of UT dependences of Doppler spectra has shown that the effects of the terminator ceased to exist either before the beginning of the solar eclipse or soon after this moment, which made the detection of the solar eclipse effects easier to perform. At the same time, an increase in $N(t)$ that followed the terminator made the response to the solar eclipse more difficult to find.

7.4 Relation between the variations observed in the Doppler spectra and the solar eclipse

7.4.1 Lintong/Pucheng to Harbin radio-wave propagation path

Figure 4 shows that the Doppler shift in the main ray exhibits a tendency to decrease from 0.8 Hz to 0.2 Hz after the solar eclipse onset. After $t > t_m$, the f_D is noted for an increase from 0.2 Hz to 0.4 Hz, and then for its reduction to the initial value. Since the analogous variations are absent on the reference days, they may be suggested to be due to the solar eclipse; most probably, an increase of 6 dBV in the signal amplitude is associated with the solar eclipse as well.

7.4.2 Chiba/Nagara to Harbin radio-wave propagation path

The Doppler shift of frequency showed a tendency to decrease from $0.2 - 0.4$ Hz to $-(0.2 - 0.4)$ Hz immediately after the solar eclipse onset, which was followed by an increase to zero, during the course of about 1 h (see Figure 5). After the moment, t_m, when the coverage of the Sun's surface area by the Moon was a maximum, i.e., when $t > t_m$, the f_D showed a tendency for an increase during 30 min. In addition, the Doppler spectra exhibited considerable, from -1.5 Hz to 1.2 Hz, broadening over the 6 January 2019 01:00 – 01:50 UT period, whereas similar effects were absent on the reference days. The effects described above may be supposed to be due to the solar eclipse.

7.4.3 Ulaanbaatar/Khonkhor to Harbin radio-wave propagation path

The rise followed by the fall in the Doppler shift observed during the 00:50 – 03:00 UT period on 6 January 2019 could be caused by the solar eclipse (see Figure 6), since analogous behavior of $f_D(t)$ was not observed within this time interval on the reference days. The diffuseness shown by the Doppler spectra from 00:50 UT to 01:25 UT on 6 January 2019 period is probably also associated with the solar eclipse.

7.4.4 Shijiazhuang to Harbin radio-wave propagation path

Figure 7 shows that $f_D \approx 0$ Hz prior to the solar eclipse onset, whereas at about 23:30 UT on 5 January 2019, the f_D exhibits an abrupt increase of 0.4 Hz, and then a tendency for 0.2 Hz reduction, which persists for about 30 min. During the following 40 min, the trend $\overline{f_D} \approx 0.2$ Hz. Around $t \approx t_m$, $\overline{f_D} \approx 0$ Hz, whereas after 00:45 UT (on 6 January 2019), the f_D exhibits an increase from 0 Hz to 0.25 Hz, and then a reduction to zero, which continue for about 12 min. The Doppler spectra show diffuseness, and the Doppler shift exhibits temporal variability from –1.5 Hz to 1.5 Hz over the 00:50 to 04:00 UT period on 6 January 2019. During the 6 January 2019 00:50 – 02:13 UT period, the second powerful enough ray was sporadically appearing with the ~0.3 Hz trend, $\overline{f_D}(t)$, whereas $\overline{f_D} \approx 0$ Hz for the first ray. Some radio wave energy was most likely leaked through the screening sporadic E layer.

The signal amplitude is observed to increase by 12 – 18 dBV during the 5/6 January 2019 night, from 23:35 to 00:50 UT, whereas on the reference days, the variations in $A(t)$ do not exceed 12 dBV. There are reasons to consider the effects described above to be due to the solar eclipse.

7.4.5 Hohhot to Harbin radio-wave propagation path

Prior to the solar eclipse onset, the Doppler shift, f_D, was nearly zero, since the radio waves were apparently reflected from the sporadic E layer (see Figure 8). At 03:40 UT on 5 January 2019, the radio wave penetrated into the ionospheric F region, and the trend $\overline{f_D} \approx 0.5$ Hz. This moment virtually coincided with the sunrise and with the onset of the observable solar eclipse. Afterwards, a gradual decrease in $\overline{f_D}$ to zero was noted to persist during a 40 min interval. Around 00:20 UT on 6 January 2019, $\overline{f_D} \approx 0$ Hz, which was followed by an increase in $\overline{f_D}$ to 0.4 Hz and by a decrease to zero at 01:30 UT on 6 January 2019. The quasi-periodic ~15 min period, T, and ~0.10 – 0.15 Hz amplitude, f_{Da}, variations were superimposed on the regular temporal variation in $\overline{f_D}(t)$. Other, weaker, rays were noted during the course of the solar eclipse and during 1 h interval after the solar eclipse.

Thus, the Doppler the spectra on the day when the solar eclipse occurred were significantly different from those observed on the reference days. The behaviors of the signal amplitudes were also significantly different. All these features support the idea that the effects described above are most likely associated with the solar eclipse. At the same time, the $f_D(t)$ dependences along all propagation paths exhibit behaviors that are significantly different from the classical behavior.

7.4.6 Beijing to Harbin radio-wave propagation path

Figures 9 and 10 show that UT dependencies of the Doppler spectra and signal amplitudes at 9,675 kHz and 9,830 kHz were observed to be virtually the same. Therefore, the use of only the first frequency is enough for the description of the effects.

Prior to the solar eclipse onset and during 1 h interval after it, the trend $\overline{f_D} \approx 0$ Hz; the radio waves were most likely reflected from the sporadic E layer. The reflection from the ionospheric F region took place only during the 5/6 January

2019 night, from 23:50 to 00:20 UT when $\overline{f_{D_{max}}}$ Hz. For this reason, the effect of the solar eclipse was masked. The appearance of rays showing the ~0.2 – 1 Hz and ~0.2 – 0.7 Hz trends, $\overline{f_D}$, over the 00:55 – 01:15 UT and 01:42 – 02:30 UT periods, respectively, are most likely associated with the solar eclipse. In addition, the $f_D(t)$ exhibited weak quasi-periodic ~4 – 5 min period, T, and ~0.05 Hz amplitude, f_{Da}, variations during all the course of the solar eclipse, whereas the ~20 min period, T, and ~0.2 Hz amplitude, f_{Da}, oscillations were predominant on the reference days.

The signal amplitude exhibited an increase of 10 – 20 dBV during the course of the solar eclipse, whereas on the reference days the increase did not exceed 5 – 10 dBV.

7.5 Results of calculations

7.5.1 Decrease in the electron density during the solar eclipse

Making use of the continuity equation for the electron density in the altitude range where the molecular ions are dominant, and taking into account the production rate that is due only to photoionization by photons from the solar disk, yields

$$\frac{N(t)}{N_0} = \sqrt{1 - B(t)}$$

where N_0 is the electron density in the absence of the solar eclipse. The value $B(t_m) = B_m$ yields the maximum effect

$$\frac{N_{min}}{N_0} = \sqrt{1 - B_m}$$

Substituting the values $B_m \approx 0.235 – 0.362$ observed at the propagation path midpoints into the latter formula yields $N_{min}/N_0 \approx 0.88 – 0.80$, $\Delta N_{max}/N_0 \approx -(12 – 20)\%$, where $\Delta N_{max} = N_{min} – N_0$.

The relations presented above could be specified by taking into account the ionization of atmospheric molecules with the ultraviolet emissions from the solar corona (Chernogor, 2013a), yielding

$$\frac{N_{min}}{N_0} = \sqrt{\frac{1 - B_m + \xi}{1 + \xi}} \tag{3}$$

where ξ is a fraction giving the relative contribution of the solar corona to the ionization of the atmosphere. According to Mrak et al. (2018), the value of ξ does not exceed 0.2, giving $\Delta N_{max}/N_0 \approx -(10–16)\%$.

7.5.2 Estimates of a decrease in the electron density from observational data

Guo et al. (2019, 2020), Luo et al. (2020), and Chernogor et al. (2020) have replaced the actual trajectory by two straightened line segments intersecting at the height of reflection z_r, ignored the geomagnetic field, and have obtained the following relation for estimating $\Delta N_{max}/N_0$, if the trend changes from $\overline{f_D}$ to $\Delta\overline{f}_{Dmax}$ during the time interval Δt:

27

$$\frac{\Delta N_{max}}{N_0} = \frac{c\Delta t}{4L_n} \frac{\kappa^2}{\kappa_\theta} \frac{\Delta \overline{f}_{D\,max}}{f}, \tag{4}$$

where $L_n = z_r - z_0$, z_r is the reflection height, z_0 is the altitude of the beginning of the layer contributing to the Doppler shift,

$$\kappa^2 = \frac{1}{1+2\zeta\tan^2\theta}, \zeta = \frac{z_r - z_0}{r_0}, \tan\theta = \frac{R}{2z_r}, \tag{5}$$

$$\kappa_\theta = \frac{\cos\theta}{1+\sin\theta} \tag{6}$$

Here $r_0 \approx 6{,}400$ km is the Earth's radius, θ is the angle of incidence with respect to the vertical at the basis of the ionosphere.

Consider, for example, the Hohhot to Harbin 9,520 kHz propagation path. The Doppler shift exhibited a maximum shift, Δf_{Dmax}, of ~–0.4 Hz during the 23:40 UT to 00:10 UT period and a minimum shift, Δf_{Dmin}, of 0.4 Hz during the 00:30 – 01:00 UT interval on the 5/6 January 2019 night. Assuming $z_r \approx 220$ km and $z_0 \approx 100$ km yields $\theta \approx 70.3°$, $L_n \approx 140$ km, whereas substituting these numbers in Eqs. (5) and (6) gives $\kappa^2 \approx 0.63$, $\kappa_\theta = 0.175$, and finally putting the latter values in Eq. (4) now yields

$$\left(\frac{\Delta N}{N_0}\right)_{max} \approx -0.15 \ .$$

This experimental estimate can be compared with the theoretical estimate. Substituting the eclipse obscuration, B_m, of ~0.293 estimated to be at the Hohhot to Harbin propagation path midpoint into Eq. (3) yields $N_{min}/N_0 \approx 0.87$, and $(\Delta N/N_0)_{max} \approx -0.13$, and hence this theoretical value shows a good agreement with the experimental estimate of –0.15 obtained as described above.

7.5.3 Estimates of wave perturbation amplitudes in the atmospheric gravity wave range

Most of the solar eclipses are well known for their capability to generate or amplify atmospheric gravity waves in the 10 – 120 min period range (see, e.g., Burmaka et al., 2006a, 2006b; Šauli et al., 2007; Chernogor, 2010, 2012, 2016a, 2016b). These waves act to excite traveling ionospheric disturbances of the same periods. Within the data segment under the study in this piece of research, oscillations in $f_D(t)$ with a period, T, of ~15 – 20 min are also observed along a number of the propagation paths.

The estimate of the relative disturbance, δ_{Na}, in the electron density at the reflection height, z_r, can be obtained from the expression analogous to Eq. (4) (Guo et al., 2019, 2020; Luo et al., 2020, Chernogor et al., 2020):

$$\delta_{Na} = \frac{cT}{4\pi L} \frac{\kappa^2}{\kappa_\theta} \frac{f_{Da}}{f} \tag{7}$$

where

28

$$L = \frac{2HL_n}{L_n + 2H} \qquad (8)$$

540 H is the scale height of the atmosphere. Assuming $2H \approx 80$ km, $L_n \approx 140$ km around the reflection height z_r, in Eq. (8) yields $L \approx 50$ km. Substituting $T \approx 15$ min and $f_{Da} \approx 0.10 - 0.15$ Hz, observed along the Hohhot to Harbin propagation path, into Eq. (7) yields $\delta_N(z_r) \approx 1.6 - 2.4\%$.

7.5.4 Estimates of wave disturbance amplitudes in the infrasound period range

Infrasound waves of great enough periods (1 – 5 min) reach the ionospheric F region altitudes, modulate the electron density
545 N, and consequently $f_D(t)$ (see, e.g., Gossard and Hooke, 1975; Guo et al., 2019, 2020; Chernogor et al., 2020).

Consider, for example, the Beijing to Harbin radio-wave propagation path. Assuming $z_r \approx 220$ km yields $\zeta = 3.4 \cdot 10^{-2}$, $\theta \approx 67.3°$, $\kappa^2 / \kappa_\theta \approx 3.59$. Substituting $L \approx 50$ km and $f_{Da} \approx 0.05$ Hz into Eq. (7) gives $\delta_N \approx 0.2 - 0.3\%$ for $T = 4 - 5$ min.

7.5.5 Comparisons with the effects from the solar eclipse of 11 August 2018 that took place in the People's Republic of
550 China

The solar eclipses of 11 August 2018 and of 5/6 January 2019 took place in the People's Republic of China. Both eclipses had close magnitudes, M, and obscurations, B_m. The effects from both eclipses were revealed with the Harbin Engineering University multi-frequency multiple path radio system.

The difference is as follows. The solar eclipse of 11 August 2018 occurred in the evening hours, whereas the solar
555 eclipse of 5/6 January 2019 was observed in the morning hours. The effects from both eclipses were partially suppressed by the processes acting at sunset or sunrise. In both cases, the solar eclipse was accompanied by Doppler spectrum broadening, alternating sign variations in Doppler shifts in the main rays, and the generation of infrasound and atmospheric gravity waves. The amplitudes of the generated waves were comparable, whereas the reductions in the electron density on a relative scale near the moment of the maximum occultation of the solar disk were observed to be 26% and 15%, respectively.

8 Conclusions
560

The results may be summarized as follows: (1) temporal variations in the Doppler spectra and Doppler shift in the main rays, as well as in the signal amplitudes observed along seven radio-wave propagation paths, with various orientations of these paths, have been studied with the Harbin engineering university multiple path multi-frequency radio system on the day of when the solar eclipse occurred and on the reference days. The transmitters located in Japan, Mongolia, and the PRC are
565 sounding the ionosphere at 5,000 kHz to 9,830 kHz frequencies.; (2) the solar eclipse was accompanied by Doppler spectrum broadening, up to ±1.5 Hz, by alternating sign Doppler shift variations, up to ±0.5 Hz, in the main ray, and by quasi-periodic

Doppler shift changes, (3) using alternating sign Doppler shift variations during the period of the maximum occultation of the Sun's surface area, the greatest decrease in the electron density has been estimated to be about –15 %, whereas the theoretical model has shown that it is –13 %, which may be considered as being in good agreement; (4) The atmospheric gravity waves launched by the solar eclipse acted to excite quasi-periodic, 15 min period variations in the Doppler shift, while the amplitude of the perturbations in the electron density has been estimated to be 1.6 – 2.4 %; and (5) the infrasound waves launched by the solar eclipse acted to excite quasi-periodic, 4–5 min period variations in the Doppler shift, whereas the amplitude of the perturbations in the electron density has been estimated to be about 0.2 – 0.3 %.

Code availability. Software for Passive 14-Channel Doppler radar may be obtained from the website at https://dataverse.harvard.edu/dataset.xhtml?persistentId=doi:10.7910/DVN/MTGAVH (Garmash, 2021).

Data availability. The data sets discussed in this paper may be obtained from the website at https://dataverse.harvard.edu/dataset.xhtml?persistentId=doi:10.7910/DVN/RMFBRN (Garmash, 2022)

Author contribution.

"**Conceptualization:** Leonid Chernogor; **Data Curation**: Qiang Guo and Kostiantyn Garmash; **Formal Analysis**: All Authors: Yu Zheng, Leonid Chernogor, Kostiantyn Garmash, Qiang Guo, Victor Rozumenko; **Funding Acquisition**: Qiang Guo; **Investigation**: Qiang Guo and Kostiantyn Garmash; **Methodology**: Leonid Chernogor; **Project Administration**: Qiang Guo; **Resources**: Qiang Guo; **Software**: Kostiantyn Garmash; **Supervision:** Leonid Chernogor; **Validation**: All Authors: Yu Zheng, Leonid Chernogor, Kostiantyn Garmash, Qiang Guo, Victor Rozumenko; **Visualization**: Kostiantyn Garmash, Yu Zheng; **Writing – original draft**: All Authors: Yu Zheng, Leonid Chernogor, Kostiantyn Garmash, Qiang Guo, Victor Rozumenko; **Writing review & editing**: All Authors: Yu Zheng, Leonid Chernogor, Kostiantyn Garmash, Qiang Guo, Victor Rozumenko.

Competing interests. The authors declare that they have no conflict of interest

600   **References**

Aa, E., Zhang, S.-R., Shen, H., Liu, S., and Li, J.: Local and conjugate ionospheric total electron content variation during the 21 June 2020 solar eclipse, Adv. Space Res., 68, 3435–3454, https://doi.org/10.1016/j.asr.2021.06.015, 2021.

Afraimovich, E.L., Voeykov, S.V., Perevalova, N.P., Vodyannikov, V.V., Gordienko, G.I., Litvinov, Yu.G., and Yakovets, A.F.: Ionospheric effects of the March 29, 2006, solar eclipse over Kazakhstan, Geomag. Aeron., 47, 461–469, 605   https://doi.org/10.1134/S0016793207040068, 2007.

Akimov, A.L., aznd Chernogor, L.F.: Effects of the Solar Eclipse of August 1, 2008 on the Earth's Lower Atmosphere, Kinemat. Phys. Celest. Bodies, 26, 135–145, https://doi.org/10.3103/S0884591310030050, 2010.

Akimov, L.A., Bogovskii, V.K., Grigorenko, E.I., Taran, V.I., and Chernogor, L.F.: Atmospheric–Ionospheric Effects of the Solar Eclipse of May 31, 2003, in Kharkov (in Russian), Geomag. Aeron., 45, 494–518, 2005.

610   Burmaka, V.P., Taran, V.I., and Chernogor, L.F.: Wave-Like Processes in the Ionosphere under Quiet and Disturbed Conditions. 1. Kharkov Incoherent Scatter Radar Observations, Geomag. Aeron., 46 (2), 183–198, https://doi.org/10.1134/S0016793206020071, 2006a.

Burmaka, V.P., Taran, V.I., and Chernogor, L.F.: Wave-Like Processes in the Ionosphere under Quiet and Disturbed Conditions. 2. Analysis of Observations and Simulation, Geomag. Aeron., 46, 199–208, 615   https://doi.org/10.1134/S0016793206020083, 2006b.

Beynon, W.J.G., and Brown, G.M. (Eds.): Solar Eclipses and the Ionosphere, Pergamon Press, London, UK, ISBN: 978-0080090467, 1956.

Chandra, H., Sethia, G., Vyas, G.D., Deshpande, M.R., and Vats, H.O.: Ionospheric effects of the total solar eclipse of 16 Feb. 1980, Proc. Indian Nat. Acad. Sci., 47, 57–60, 1980.

620   Chapman, S.: The influence of a solar eclipse upon the upper atmospheric ionization, Mon. Not. R. Astron. Soc., 92, 413–420, 1932.

Chen, Y., Feng, P., Liu, C., Chen, Y., Huang, L., Duan, J., Hua, Y., and Li, X.: Impact of the annular solar eclipse on June 21, 2020 on BPL time service performance, AIP Advances, 11, id: 115003, https://doi.org/10.1063/5.0064445, 2021.

Chernogor, L.F.: Physics of Earth, Atmosphere, and Geospace from the Standpoint of System Paradigm (in Russian), Radio 625   Phys. Radio Astron., 8, 59–106, http://rpra-journal.org.ua/index.php/ra/article/view/797, 2003.

Chernogor, L.F.: Variations in the Amplitude and Phase of VLF Radiowaves in the Ionosphere during the August 1, 2008, Solar Eclipse, Geomag. Aeron., 50, 96–106, https://doi.org/10.1134/S0016793210010111, 2010.

Chernogor, L.F.: Wave Response of the Ionosphere to the Partial Solar Eclipse of August 1, 2008, Geomag. Aeron., 50, 346–361, https://doi.org/10.1134/S0016793210030096, 2010.

630   Chernogor, L.F.: The Earth–atmosphere–geospace system: main properties and processes, Int. J. Rem. Sens., 32, 3199–3218, https://doi.org/10.1080/01431161.2010.541510, 2011.

Chernogor, L.F.: Effects of solar eclipses in the ionosphere: Results of Doppler sounding: 1. Experimental data, Geomag. Aeron., 52, 768–778, https://doi.org/10.1134/S0016793212050039, 2012a.

Chernogor, L.F.: Effects of Solar Eclipses in the Ionosphere: Doppler Sounding Results: 2. Spectral Analysis, Geomag.

635   Aeron., 52, 779–792,https://doi.org/10.1134/S0016793212050040, 2012b.

Chernogor, L.F.: Physical Effects of Solar Eclipses in Atmosphere and Geospace: monograph (in Russian), V. N. Karazin Kharkiv National University Publ., Kharkiv, Ukraine, 2013a.

Chernogor, L.F.: Physical Processes in the Middle Ionosphere Accompanying the Solar Eclipse of January 4, 2011, in Kharkov, Geomag. Aeron., 53, 19–31, https://doi.org/10.1134/S0016793213010052, 2013b.

640   Chernogor, L.F.: Atmosphere–Ionosphere response to Solar Eclipse over Kharkiv on March 20, 2015, Geomag. Aeron., 56, 592–603, https://doi.org/10.1134/S0016793216050030, 2016a.

Chernogor, L.F.: Wave Processes in the Ionosphere over Europe that Accompanied the Solar Eclipse of March 20, 2015, Kinemat. Phys. Celest. Bodies, 32, 196–206, https://doi.org/10.3103/S0884591316040024, 2016b.

Chernogor, L.F.: Convection Effect in the Surface Atmosphere of Solar Eclipses of March 20, 2015, and June 10, 2021,

645   Kinemat. Phys. Celest. Bodies, 37, 284–292, https://doi.org/10.3103/S0884591321060039, 2021*a*.

Chernogor, L.F.: Thermal Effect in Surface Atmosphere of the Solar Eclipse on June 10, 2021, Kinemat. Phys. Celest. Bodies, 37, 293–299, https://doi.org/10.3103/S0884591321060040, 2021*b*.

Chernogor, L.F.: Geomagnetic Effect of the Solar Eclipse of June 10, 2021, Kinemat. Phys. Celest. Bodies, 38, 11–24, https://doi.org/10.3103/S0884591322010020, 2022.

650   Chernogor, L.F. and Rozumenko, V.T.: Earth – Atmosphere – Geospace as an Open Nonlinear Dynamical System, Radio Phys. Radio Astron., 13, 120–137. http://rpra-journal.org.ua/index.php/ra/article/view/563, 2008.

Chernogor, L.F. and Garmash, K.P.: Magneto-Ionospheric Effects of the Solar Eclipse of March 20, 2015, over Kharkov, Geomag. Aeron., 57, 72–83, https://doi.org/10.1134/S0016793216060062, 2017.

Chernogor, L.F. and Mylovanov, Yu.B.: Ionospheric Effects from the June 10, 2021 Solar Eclipse in the Polar Region.

655   Kinemat. Phys. Celest. Bodies., in press, 2022.

Chernogor, L.F. and Garmash, K.P.: Ionospheric Processes during the Partial Solar Eclipse above Kharkiv on June 10, 2021, Kinemat. Phys. Celest. Bodies, 38, 61–72, 2022.

Chernogor, L.F., Garmash, K.P., Guo, Q., Rozumenko, V.T., Zheng, Y., and Luo, Y.: Supertyphoon Hagibis action in the ionosphere on 6–13 October 2019: Results from multi-frequency multiple path sounding at oblique incidence, Adv. Space

660 Res., 67, 2439–2469, https://doi.org/10.1016/j.asr.2021.01.038, 2021.

Chernogor, L.F., Garmash, K.P., Guo, Q., Rozumenko, V.T., Zheng, Y., and Luo, Y.: Disturbances in the Ionosphere That Accompanied Typhoon Activity in the Vicinity of China in September 2019, Radio Sci., 57, Paper No. e2022RS007431, https://doi.org/10.1029/2022RS007431, 2022.

Chernogor, L.F., Domnin, I.F., Emelyanov, L.Ya., and Lyashenko, M.V.: Physical processes in the ionosphere during the

665 solar eclipse on March 20, 2015 over Kharkiv, Ukraine (49.6°N, 36.3°E), J. Atmos. Solar-Terr. Phys., 182, 1–9, https://doi.org/10.1016/j.jastp.2018.10.016, 2019.

Chernogor, L.F., Garmash, K.P., Guo, Q., Luo, Y., Rozumenko, V.T., and Zheng, Y.: Ionospheric storm effects over the People's Republic of China on 14 May 2019: Results from multipath multi-frequency oblique radio sounding, Adv. Space Res., 66, 226–242, https://doi.org/10.1016/j.asr.2020.03.037, 2020.

670 Chernogor L. F., Garmash K. P., Guo Q., Rozumenko V. T., Zheng Y., and Luo Y.: Supertyphoon Hagibis action in the ionosphere on 6–13 October 2019: Results from multi-frequency multiple path sounding at oblique incidence, Adv. Space Res., 67, 2439–2469, https://doi.org/10.1016/j.asr.2021.01.038, 2021.

Chimonas, G. and Hines, C.O.: Atmospheric gravity waves induced by a solar eclipse, J. Geophys. Res., 75, 875–876, https://doi.org/10.1029/JA075i004p00875, 1970.

675 Coster, A.J., Goncharenko, L., Zhang, S.R., Erickson, P.J., Rideout, W., and Vierinen, J.: GNSS observations of ionospheric variations during the 21 August 2017 solar eclipse, Geophys. Res. Lett., 44, 12041–12048, https://doi.org/10.1002/2017GL075774, 2017.

Dang, T., Lei, J.H., Wang, W.B., Yan, M.D., Ren, D.X., and Huang, F.Q.: Prediction of the thermospheric and ionospheric responses to the 21 June 2020 annular solar eclipse, Earth Planet. Phys, 4, 231–237, https://doi.org/10.26464/epp2020032,

680 2020.

Davies, K.: Ionospheric Radio, Peter Peregrinus Ltd., London, UK, http://dx.doi.org/10.1049/PBEW031E, 1990.

Deshpande, M.R., Chandra, H., Sethia, G., Vats, Hari Om, Vyas, G.D., Iyer, K.N., and Janve, A.V.: Effects of the total solar eclipse of 16 February 1980 on TEC at low latitudes, Proc. Indian. Nat. Acad. Sci., A48, 427–433, 1982.

Eclipse Supplement, Nature, 226, 1097–1155, 1970.

685 Founda, D., Melas, D., Lykoudis, S., Lisaridis, I., Gerasopoulos, E., Kouvarakis, G., Petrakis, M., and Zerefos, C.: The effect of the total solar eclipse of 29 March 2006 on meteorological variables in Greece, Atmos. Chem. Phys., 7, 5543–5553, https://doi.org/10.5194/acp-7-5543-2007, 2007.

Garmash, K.P., Leus, S.G., and Chernogor, L.F.: January 4, 2011 Solar Eclipse Effects over Radio Circuits at Oblique Incidence (in Russian), Radio Phys. Radio Astron., 16, 164–176, http://rpra-journal.org.ua/index.php/ra/article/view/442,

690 2011.

Garmash, K.: RAW Data for Solar Eclipse of January 5–6, 2019 over China, https://dataverse.harvard.edu/dataset.xhtml?persistentId=doi:10.7910/DVN/RMFBRN, Harvard Dataverse, V1, (2022)

Garmash, K.: Software for Passive 14-Channel Doppler Radar, Harvard Dataverse, V1, https://doi.org/10.7910/DVN/MTGAVH, (2021).

695 Gossard, E.E. and Hooke, W.H.: Waves in the Atmosphere, vol. 456, Elsevier, New York, 1975.

Grigorenko, E.I., Lyashenko, M.V., and Chernogor, L.F.: Effects of Solar Eclipse of March 29, 2006, in the Ionosphere and Atmosphere, Geomag. Aeron., 48 (3), 337–351, https://doi.org/10.1134/S0016793208030092, 2008.

Guo, Q., Chernogor, L.F., Garmash, K.P., Rozumenko, V.T., and Zheng, Y.: Dynamical processes in the ionosphere following the moderate earthquake in Japan on 7 July 2018, J. Atmos. Solar-Terr. Phys., 186, 88 – 103,

700 https://doi.org/10.1016/j.jastp.2019.02.003, 2019.

Guo, Q., Chernogor, L.F., Garmash, K.P., Rozumenko, V.T., and Zheng, Y.: Radio Monitoring of Dynamic Processes in the Ionosphere Over China During the Partial Solar Eclipse of 11 August 2018, Radio Sci., 55, e2019RS006866, https://doi.org/10.1029/2019RS006866, 2020.

Higgs, A.J.: Ionospheric measurements made during the total Solar eclipse of 1940, October 1-st, South Africa, Monthly Not.

705 Roy. Astron. Soc., 102, 24–34, https://doi.org/10.1093/mnras/102.1.24, 1942.

Huang, L., Liu, C., Chen, Y., Wang, X., Feng, P., and Li, X.: Observations and analysis of the impact of annular eclipse on 10 MHz short-wave signal in Sanya area on June 21, 2020, AIP Adv., 11, id: 115317, https://doi.org/10.1063/5.0068778, 1942.

Huang, F., Li, Q., Shen, X., Xiong, C., Yan, R., Zhang, S.-R., Wang, W., Aa, E., Zhong, J., Dang, T., and Lei, J.:

710 Ionospheric responses at low latitudes to the annular solar eclipse on 21 June 2020, J. Geophys. Res., 125, id:e2020JA028483. https://doi.org/10.1029/2020JA028483, 2020.

Jakowski, N., Stankov, S.M., Wilken, V., Borries, C., Altadill, D., Chum, J., Buresova, D., Boska, J., Sauli, P., Hruska, F., and Cander, Lj.R.: Ionospheric behavior over Europe during the solar eclipse of 3 October 2005, J. Atmos. Sol.-Terr. Phys., 70, 836–853, https://doi.org/10.1016/j.jastp.2007.02.016, 2008.

715 Le, H., Liu, L., Ren, Z., Chen, Y., and Zhang, H.: Effects of the 21 June 2020 solar eclipse on conjugate hemispheres: A modeling study, J. Geophys. Res., 125, Article id:e2020JA028344, https://doi.org/10.1029/2020JA028344, 2020.

Liu, J.Y., Hsiao, C.C., Tsai, L.C., Liu, C.H., Kuo, F.S., Lue, H.Y., and Huang, C.M.: Vertical phase and group velocities of internal gravity waves derived from ionograms during the solar eclipse of 24 October 1995, J. Atmos. Sol.-Terr. Phys., 60, 1679–1686, https://doi.org/10.1016/S1364-6826(98)00103-5, 1998.

720 Luo, Y., Chernogor, L.F., Garmash, K.P., Guo, Q., Rozumenko, V.T., Shulga, S.N., and Zheng, Y.: Ionospheric effects of the Kamchatka meteoroid: Results from multipath oblique sounding, J. Atmos. Solar-Terr. Phys., 207, Paper No. 105336, https://doi.org/10.1016/j.jastp.2020.105336, 2020.

Lyashenko, M.V. and Chernogor, L.F.: Tropospheric-ionospheric effects of the 3 October 2005 partial solar eclipse in Kharkiv. 2. Modeling and discussion (in Russian), Space Sci Tech., 14, 57–64, https://doi.org/10.15407/knit2008.01.057,

725 2008.

Marlton, G.J., Williams, P.D., and Nicoll, K.A.: On the detection and attribution of gravity waves generated by the 20 March 2015 solar eclipse, Phil. Trans. R. Soc. A, 374, http://dx.doi.org/10.1098/rsta.2015.0222, 2016.

Marple Jr., S. L.: Digital Spectral Analysis: with Applications, Prentice-Hall, Inc, Englewood Cliffs, N. J., https://doi.org/10.1121/1.398548, 1987.

730   Mrak, S., Semeter, J.L., Drob, D., and Huba, J.D.: Direct EUV/X-ray modulation of the ionosphere during the August 2017 total solar eclipse. Geophys. Res. Let., 45, 3820–3828. https://doi.org/10.1029/2017GL076771, 2018.

Özcan, O., and Aydoğdu, M.: Possible effects of the total solar eclipse of August 11, 1999 on the geomagnetic field variations over Elaziğ-Turkey, J. Atmos. Solar-Terr. Phys., 66, 997–1000, DOI:10.1016/j.jastp.2004.03.009, 2004.

Panasenko, S.V., Otsuka, Y., van de Kamp, M., Chernogor, L.F., Shinbori, A., Tsugawa, T., and Nishioka, M.: Observation

735   and characterization of traveling ionospheric disturbances induced by solar eclipse of 20 March 2015 using incoherent scatter radars and GPS networks, J. Atmos. Solar-Terr. Phys., 191, Article No. 105051, https://doi.org/10.1016/j.jastp.2019.05.015, 2019.

Patel, K. and Singh, A.K.: Changes in atmospheric parameters due to annular solar eclipse of June 21, 2020, over India, Indian J. Phys., https://doi.org/10.1007/s12648-021-02112-2, 2021.

740   Rama Rao, P.V.S., Rao, B.V.P.S., Nru, D., and Niranjan, K.: TEC observations at Waltair during the total solar eclipse of 16 Februrary 1980, Proc. Indian Nat. Acad. Sci., 48, 434–438, 1982.

Roble, R.G., Emery, B.A., and Ridley, E.C.: Ionospheric and thermospheric response over Millstone Hill to the May 30, 1984, annular solar eclipse, J. Geophys. Res., 91, 1661–1670, https://doi.org/10.1029/JA091iA02p01661, 1986.

Salah, J.E., Oliver, W.L., Foster, J.C., Holt, J.M., Emery, B.A., and Roble, R.G.: Observations of the May 30, 1984, annular

745   solar eclipse at Millstone Hill, J. Geophys. Res., 91, 1651–1660, https://doi.org/10.1029/JA091iA02p01651, 1986.

Šauli, P., Roux, S.G., Abry, P., and Boška, J.: Acoustic–gravity waves during solar eclipses: Detection and characterization using wavelet transforms, J. Atmos. Sol.-Terr. Phys., 69, 2465–2484, https://doi.org/10.1016/j.jastp.2007.06.012, 2007.

Sen Gurta, A., Goel, G.K., and Mathur, B.S.: Effect of the 16 February 1980 solar eclipse on VLF propagation, J. Atmos. Terr. Phys., 42, 907–909, https://doi.org/10.1016/0021-9169(80)90107-5, 1980.

750   Şentürk, E., Arqim Adil, M., and Saqib, M.: Ionospheric total electron content response to annular solar eclipse on June 21, 2020, Adv. Space Res., 67, 1937–1947, https://doi.org/10.1016/j.asr.2020.12.024, 2021.

Shagimuratov, I.I., Zakharenkova, I.E., Tepenitsyna, N.Y., Yakimova, G.A., and Efishov, I.I.: Features of the Ionospheric Total Electronic Content Response to the Annular Solar Eclipse of June 21, 2020, Geomagn. Aeron., 61, 756–762, https://doi.org/10.1134/S001679322105011X, 2021.

755   Journal of Atmospheric and Terrestrial Physics, 34, Issue 4, 559–745, https://www.sciencedirect.com/journal/journal-of-atmospheric-and-terrestrial-physics/vol/34/issue/4, 1972.

Anastassiades, M. (Ed): Solar Eclipses and the Ionosphere, Plenum Press, New York, 1970.

Stankov, S.M., Bergeot, N., Berghmans, D., Bolsée, D., Bruyninx, C., Chevalier, J.M., Clette, F., De Backer, H., De Keyser, J., D'Huys, E., Dominique, M., Lemaire, J.F., Magdalenić, J., Marqué, C., Pereira, N., Pierrard, V., Sapundjiev, D., Seaton,

D.B., Stegen, K., Linden, R.V., Verhulst, T.G.W., and West, M.J.: Multi-instrument observations of the solar eclipse on 20 March 2015 and its effects on the ionosphere over Belgium and Europe, J. Space Weather Space Clim., 7, Article No. A19, http://dx.doi.org/10.1051/swsc/2017017, 2017.

Sun, Y.-Y., Chen, C.-H., Qing, H., Xu, R., Su, X., Jiang, C., Yu, T., Wang, J., Xu, H., and Lin, K.: Nighttime ionosphere perturbed by the annular solar eclipse on June 21, 2020, J. Geophys. Res., 126, id:e2021JA029419, https://doi.org/10.1029/2021JA029419, 2021.

Tripathi, G., Singh, S.B., Kumar, S., Ashutosh, K., Singh Singh, R., and Singh, A.K.: Effect of 21 June 2020 solar eclipse on the ionosphere using VLF and GPS observations and modeling, Adv. Space Res., 69, 254–265, https://doi.org/10.1016/j.asr.2021.11.007, 2022.

EclipseWise.com: http://www.eclipsewise.com/solar/SEprime/2001-2100/SE2019Jan06Pprime.html/ last access: 02 May 2022.

Uryadov, V.P., Leonov, A.M., Ponyatov, A.A., Boiko, G.N., and Terent'ev, S.P.: Variations in the Characteristics of a HF Signal over an Oblique Sounding Path during the Solar Eclipse on August 11, 1999, Radiophys. Quant. El., 43, 614–618, https://doi.org/10.1023/A:1004801201847, 2000.

Uryadov, V.P., Kolchev, A.A., Vybornov, F.I., Shumaev, V.V., Egoshin, A.I., and Chernov, A.G.: Ionospheric effects of a solar eclipse of March 20, 2015 on oblique sounding paths in the Eurasian longitudinal sector, Radiophys. Quantum Electron., 59, 431–441, https://doi.org/10.1007/s11141-016-9711-9, 2016.

Verhulst, T.G.W., Sapundjiev, D., and Stankov, S.M.: High-resolution ionospheric observations and modeling over Belgium during the solar eclipse of 20 March 2015 including first results of ionospheric tilt and plasma drift measurements, Adv. Space Res., 57, 2407–2419, https://doi.org/10.1016/j.asr.2016.03.009, 2016.

Verhulst, T.G.W. and Stankov, S.M.: Height dependency of solar eclipse effects: the ionospheric perspective. J. Geophys. Res.: Space Phys., 125, e2020JA028088, https://doi.org/10.1029/2020JA028088 , 2020.

Wang, X., Li, B., Zhao, F., Luo, X., Huang, L., Feng, P., and Li, X.: Variation of Low-Frequency Time-Code Signal Field Strength during the Annular Solar Eclipse on 21 June 2020: Observation and Analysis, Sensors, 21, id: 1216, https://doi.org/10.3390/s21041216, 2021*a*.

Wang, J., Zuo, X., Sun, Y.-Y., Yu, T., Wang, Y., Qiu, L., Mao, T., Yan, X., Yang, N., Qi, Y., Lei, J., Sun, L., and Zhao, B.: Multilayered sporadic-E response to the annular solar eclipse on June 21, 2020, Space Weather, 19, id:e2020SW002643, https://doi.org/10.1029/2020SW002643, 2021*b*.

Zhang, R., Le, H., Li, W., Ma, H., Yang, Y., Huang, H., Li, Q., Zhao, X., Xie, H., Sun, W., Li, G., Chen, Y., Zhang, H., and Liu, L.: Multiple technique observations of the ionospheric responses to the 21 June 2020 solar eclipse, J. Geophys. Res., 125, id:e2020JA028450, https://doi.org/10.1029/2020JA028450, 2020.